A phenotype-based forward genetic screen identifies *Dnajb6* as a sick sinus syndrome gene

Yonghe Ding[1,2], Di Lang[3], Jianhua Yan[1,4], Haisong Bu[1,5], Hongsong Li[1,6], Kunli Jiao[1,4], Jingchun Yang[1], Tai Le[7], Karl J. Clark[8], Stephen C. Ekker[8], Hung Cao[7,9], Yuji Zhang[10], Yigang Li[4], Alexey V. Glukhov [3], Xiaolei Xu[1*]

[1]Department of Biochemistry and Molecular Biology, Department of Cardiovascular Medicine, Mayo Clinic, Rochester, MN, USA; [2]The Affiliated Hospital of Qingdao University & The Biomedical Sciences Institute of Qingdao University (Qingdao Branch of SJTU Bio-X Institutes), Qingdao University, Qingdao, China; [3]Department of Medicine, School of Medicine and Public Health, University of Wisconsin-Madison, Madison, WI, USA; [4]Division of Cardiology, Xinhua Hospital Affiliated to Shanghai Jiaotong University School Of Medicine, Shanghai, China; [5]Department of Cardiothoracic Surgery, Xiangya Hospital, Central South University, Changsha, China; [6]Department of Cardiovascular Medicine, Jiading District Central Hospital Affiliated Shanghai University of Medicine & Health Science, Shanghai, China; [7]Department of Electrical Engineering and Computer Science, University of California Irvine, Irvine, CA, USA; [8]Department of Biochemistry and Molecular Biology, Mayo Clinic, Rochester, MN, USA; [9]Department of Biomedical Engineering, University of California Irvine, Irvine, CA, USA; [10]Department of Epidemiology and Public Health, University of Maryland School of Medicine, Baltimore, Maryland, USA.

*** For correspondence:**

Xiaolei Xu, PhD, Professor of Biochemistry and Molecular Biology, Department of Biochemistry and Molecular Biology, Department of Cardiovascular Medicine, Mayo Clinic College of Medicine, Rochester, MN 55905. E-mail: xu.xiaolei@mayo.edu

Running title: Sick sinus syndrome associated genes identification

Key words: Sinus arrest; Sick sinus syndrome; Dnajb6; Electrocardiogram; Zebrafish.

Abstract

Sick sinus syndrome (SSS) is a group of heart rhythm disorders caused by malfunction of the sinus node, the heart's primary pacemaker. Partially owing to its aging-associated phenotypic manifestation and low expressivity, molecular mechanisms of SSS remain difficult to decipher. Here, we aim to develop a phenotype-based forward genetic approach in the zebrafish (*Danio rerio*) animal model for discovering essential genes which dysfunction could result in SSS-like phenotypes. Previously we showed the generation of protein trap library by using a revertible gene-breaking transposon (GBT)-based insertional mutagenesis system. Here, we reported the generation of a collection of 35 zebrafish insertional cardiac lines derived from this protein trap library, which was screened using electrocardiographic measurements. As a result, three mutants with SSS-like phenotypes were identified. We then focused on one of these 3 GBT mutants called *GBT411* in which *dnajb6b* gene was disrupted, and conducted expressional, genetic, transcriptome, and electrophysiological studies using both zebrafish and mouse models. These studies confirmed the identity of *Dnajb6* as a novel SSS causative gene with a unique expression pattern within the specialized population of sinus node pacemaker cardiomyocytes that lack the expression of HCN4 channels. Together, this study demonstrates the feasibility of a genetic screening approach in an adult vertebrate animal model for discovering new genetic factors for a heart rhythm disorder such as SSS.

1. Introduction

Cardiac arrhythmia affects >2% of individuals in community-dwelling adults.[1] Sick sinus syndrome (SSS), also known as sinus node dysfunction or sinoatrial node (SAN) disease, is a group of heart rhythm disorders affecting cardiac impulse formation and/or propagation from the SAN, the heart's primary pacemaker. SSS manifests a spectrum of presentations such as sinus pause or arrest (SA), bradycardia, sinoatrial exit block, or tachy-brady syndrome accompanied by atrial fibrillation (AF).[2, 3] In addition, 20% to 60% SSS patients show abnormal response to autonomic stresses.[4] SSS occurs most commonly in elderly, with an estimated prevalence of 1 case per 600 adults over age 65. Symptomatic SSS can lead to inadequate blood supply to the heart and body and contribute significantly to life-threatening problems such as heart failure and cardiac arrest. While SSS is the most common indication for pacemaker implantation worldwide,[5] the mechanisms of SSS remain poorly understood, making it difficult to stratify SSS risk in vulnerable cohorts of patients and development of effective pharmacologic therapy for pacemaker abnormalities.

To develop mechanism-based diagnostic and therapeutic strategies for SSS, it is desirable to discover genes that are expressed in the SAN and may contribute to SSS. Unfortunately, very limited number of SSS genes and related animal models are currently available. While mutations in the cardiac sodium channel α-subunit encoding gene (*SCN5A*) [6, 7] and hyperpolarization-activated cyclic nucleotide-aged channel encoding gene (*HCN4*) [8, 9] have been found to cause SSS, only a few other genes affecting the structure and/or function of the SAN were identified to increase the risk of developing SSS.[10, 11] Classic human genetic

72 linkage analysis-based approach has played important roles in gene discovery, but it is
73 largely limited by the availability of suitable pedigree, especially in this age-dependent
74 disease.[12] More recently, the genome-wide association studies (GWASs) have been used to
75 identify novel genetic susceptibility factors associated with SSS.[11, 13] However, owing to its
76 statistic and associative nature, it has been difficult to confidently establish genotype-
77 phenotype relationships for the vast amount of variants.[14, 15] Alternative approaches for
78 effective identification of essential genes for SSS are thus needed.

79 Phenotype-based forward genetic screen in model organisms is a powerful strategy for
80 deciphering genetic basis of a biological process. Without any *a prior* assumption, new
81 genes can be identified that shed light on key signaling pathways. However, this approach is
82 difficult to carry out in adult vertebrates, because of significantly increased burden of colony
83 management efforts.[16, 17] To address this bottleneck, zebrafish, a vertebrate with higher
84 throughput than rodents, has been explored to study cardiac diseases.[18] Despite its small
85 body size, a zebrafish heart has conserved myocardium, endocardium, and epicardium as
86 found in human, and adult zebrafish shows strikingly similar cardiac physiology to humans.[19]
87 Its heart rate is around 100 beats per minute (bpm), which is much comparable to that in
88 human than in rodents. Adult zebrafish models for human cardiac diseases such as
89 cardiomyopathies have been successfully generated.[20] Besides *N*-ethyl-*N*-nitrosourea
90 (ENU)-based mutagenesis screens that have been conducted to identify embryonic
91 recessive mutants, insertional mutagens such as those based on viruses and/or transposons
92 have been developed to further increase the throughput of the screen, opening doors to

93 screening genes affecting adult phenotypes.[21, 22] Our team recently reported a gene-
94 breaking transposon (GBT)-based gene-trap system in zebrafish which enables to disrupt
95 gene function reversibly at high efficiency (>99% at the RNA level).[23] Approximately 1,200
96 GBT lines have been generated, laying a foundation for adult phenotype-based forward
97 genetic screens.[24] Because the expression pattern of the affected genes in each GBT line is
98 reported by a fluorescence reporter, we enriched GBT lines with cardiac expression and
99 generated a zebrafish insertional cardiac (ZIC) mutant collection.[25] Through stressing the
100 ZIC collection with doxorubicin, an anti-cancer drug, we demonstrated that novel genetic
101 factors of doxorubicin-induced cardiomyopathy (DIC), such as Dnaj (Hsp40) homology,
102 subfamily B, member 6b (*dnajb6b*), sorbin and SH3 domain-containing 2b (*sorbs2b*) and
103 retinoid x receptor alpha a (*rxraa*), could be successfully identified.[26-28] Follow up studies on
104 these hits confirmed their identity as important cardiomyopathy genes.

105 Encouraged by our success in identifying new genetic factors for DIC, we reasoned that
106 genes for rhythm disorders could be similarly identified by directly screening adult ZIC lines
107 using echocardiographic measurement. We had recently optimized a commercially available
108 ECG system to define SA episodes in an adult zebrafish, and the baseline frequency of
109 aging-associated SSS in wild-type (WT) adult zebrafish.[29] Here, we reported a pilot screen of
110 our ZIC collection using this ECG platform and the resultant discovery of 3 positive hits,
111 followed by comprehensive expressional and functional analysis of *dnajb6b* gene that is
112 linked to one of the hits. Together, our data prove the feasibility of a phenotype-based
113 screening strategy in adult zebrafish for discovering new rhythm genes.

2. Results

2.1 Identification of 35 zebrafish insertional cardiac (ZIC) mutants

We recently reported the generation of more than 1,200 zebrafish mutant strains using the gene-break transposon (GBT) vector.[24] The tagged gene in each GBT mutant is typically disrupted with 99% knockdown efficiency and its expression pattern is reported by a monomeric red fluorescent protein (mRFP) reporter.[24] We screened 609 GBT lines based on their mRFP expression and identified 44 mutants with either the embryonic or adult heart expression.[26] Then, we outcrossed these 44 lines, aided by Southern blotting to identify offsprings with a lower copy number of insertions,[25] and identified 35 mutants with a single copy of the GBT insertion after 2-4 generations of outcross (Table 1).[26] Using a combination of inverse PCR and/or 5'- and 3'-RACE PCR cloning approaches, we mapped the genetic loci of GBT inserts in these 35 mutants (Table 1).[25] A majority of the affected genes have human orthologs with a corresponding Online Mendelian Inheritance in Man (OMIM) number. Because each GBT line contains a single GBT insertion that traps a gene with cardiac expression, these 35 GBT lines were termed as zebrafish insertional cardiac (ZIC) mutants.

2.2 An ECG screen of 35 ZIC lines identified 3 mutants with increased incidence of SA and/or AV block episodes

Because each ZIC mutant disrupts a gene with cardiac expression, we enquired whether an ECG screening can be conducted to identify genetic lesions that result in arrhythmia. Since aging is a strong risk factor for heart rhythm disorders, we carried our screen in fish aged

135 from 1.5 to 2 years old to facilitate the manifestation of cardiac rhythm abnormalities.
136 Because these fish are offsprings of incrosses and have been preselected based on the
137 RFP tag, their genotype consists of both heterozygous and homozygous for the affected
138 genes. In WT fish aged around 2 years old, we noted baseline SA episodes in about 1 out
139 of 20 fish (5%) fish.[29] By contrast, among the 35 ZIC lines, we noted a significantly increased
140 incidence of SA in 3 lines, including 3 out of 13 *GBT103* fish at 1.5 years old, 4 out of 10
141 *GBT410* fish at 2 years old, and 3 out of 8 *GBT411* fish at 2 years old (Figure 1A). In
142 addition to SA, we also noted incidence of atrioventricular block (AVB) in 4 out of 13 *GBT103*
143 fish at 1.5 years of age. Because the increased incidence of SA and/or AVB is hallmark of
144 SSS, these 3 lines were thus identified as 3 candidate SSS-like mutants.

145 To confirm the linkage between genetic lesions and the SSS-like phenotypes, we
146 incrossed these 3 ZIC mutants to obtain homozygous animals. This is possible because the
147 precise insertional positions for all the 35 ZIC lines have been mapped (Table 1, Figure 1B).
148 We carried genotyping PCR to identify homozygous mutants for the 3 candidate ZIC lines
149 using genomic DNA isolated from their tail fins, raised up homozygous fish to 16 months,
150 and carried out ECG assays at room temperature (25 °C). In contrast to 5% WT fish
151 whereby SA episodes can be detected, significantly increased SA incidence was noted in all
152 3 homozygous mutants, with an incidence of 57.1% in the *GBT103/cyth3a*, 44.4% in the
153 *GBT410/vapal*, and 40% in the *GBT411/dnajb6b* mutant, respectively (Table 2). We also
154 noted a reduced heart rate, another SSS phenotypic trait in the *GBT411*$^{-/-}$ homozygous, but
155 not the other two GBT homozygous mutants (Table 2).

156 To seek additional evidence supporting our screening strategy, we decided to focus on
157 the *GBT411/dnajb6b* mutant that is the most arrhythmogenic – this mutant is also
158 characterized with reduced heart rate phenotype. Because arrhythmic mutants often
159 manifest an aberrant response to extrinsic regulation of the heart rate, we examined
160 responses of the *GBT411/dnajb6b* homozygous mutants (*GBT411*$^{-/-}$) to autonomic stimuli by
161 stressing them with 3 compounds, including isoproterenol, a β-adrenoreceptor agonist for
162 sympathetic nervous system; atropine, an anticholinergic inhibitor; and carbachol, a
163 cholinergic agonist for parasympathetic nervous system. After administrating these drugs to
164 the *GBT411*$^{-/-}$ fish at 1 year old via intraperitoneal (IP) injection, we noted aberrant heart rate
165 response to both atropine and carbachol, while its response to isoproterenol remained
166 unchanged (Supplemental Figure 1). Next, we stressed the *GBT411*$^{-/-}$ fish with verapamil, an
167 L-type Ca^{2+} channel antagonists, to stress out cardiac pacemaking and unmask SSS
168 phenotype. Indeed, SA incidence was significantly increased in the *GBT411*$^{-/-}$ fish at 10
169 months of age (Supplemental Table 1). Similarly, the heart rate was significantly reduced in
170 the *GBT411*$^{-/-}$ fish compared to WT controls. Together, these data provided additional
171 evidence to support *GBT411/dnajb6b* as an arrhythmia mutant.

172 **2.3 Dnajb6 expression is enriched in the SAN tissue, manifesting a unique expression**
173 **pattern**

174 *Dnajb6* was previously identified as a cardiomyopathy-associated gene,[26] raising concerns
175 on whether the arrhythmic phenotype in the *GBT411/dnajb6b* mutant is a primary defect in
176 the cardiac conduction system or a consequence of cardiac remodeling in cardiomyocytes.

177 To address this further, we firstly defined the expression of the Dnajb6 protein in the heart.
178 Our previous characterization of the mRFP reporter in the *GBT411/dnajb6b* fish revealed
179 expression of Dnajb6b protein in both the embryonic and the adult hearts.[25, 26] To enquire its
180 expression in the cardiac conduction system (CCS), we crossed the *GBT411/dnajb6b* line
181 into the sqET33-mi59B transgenic line in which EGFP labels the zebrafish SAN and atrio-
182 ventricular canal (AVC) cells.[30] Co-localization analysis demonstrated that the mRFP
183 positive, Dnajb6b-expressing cells partially overlap with the EGFP signal labeling SAN cells
184 at the base of atrium in the embryonic heart at 3 days post-fertilization and also AVC in adult
185 heart tissues (Figure 2A and 2B). It should be noted that the Dnajb6b-mRFP-positive
186 expression patterns overlap with but extend beyond the sqET33-mi59B EGFP-positive
187 expression patterns in both embryonic and adult fish hearts (Figure 2A and 2B).

188 To seek additional evidence supporting expression and function of Dnajb6 in the CCS,
189 we turned to the mouse model, and noted Dnajb6 protein expression in all 4 cardiac
190 chambers in a sectioned mouse heart tissue (Supplemental Figure 2). Interestingly, we
191 found a highly enriched expression of Dnajb6 specifically in the SAN region, as indicated by
192 its localization in the region with expression of HCN4 channel which are responsible for the
193 generation of hyperpolarization-activated pacemaker “funny” current in pacemaker cells
194 (Figure 2C). However, at higher magnification images, only a small proportion of Dnajb6-
195 positive cells showed colocalization with the HCN4-positive cells (arrows for colocalized cells
196 vs. arrowheads non-colocalized cells in Figure 2D). In addition, we noted co-localization of
197 Dnajb6 with Tbx3 and Islet1, two transcription factors that specify the formation of the SAN

198 cells.[32] Interestingly, we found a negative correlation between Dnajb6 and Tbx3 expression
199 levels: cells with strong Dnajb6 expression tend to overlap with cells that show weak Tbx3
200 signal, while cells with weak Dnajb6 expression tend to overlap with the cells with strong
201 Tbx3 signal. In contrast, the Dnajb6 expressing cells largely overlap with the Islet1 positive
202 cells. In summary, the enriched expression of Dnajb6 in the SAN region may indicate that
203 Dnajb6 could contribute to SSS development; however, its unique expression patterns
204 underscored heterogeneity of pacemaker cells within the SAN.[33, 34]

205 **2.4 The *Dnajb6*$^{+/-}$ mice manifest features of SSS when there is no sign of**
206 **cardiomyopathy**

207 To test the conservation of the cardiac arrhythmic functions of dnajb6 suggested from
208 zebrafish, we obtained a global *Dnajb6* knock out (KO) mouse line. The mutant harbors a
209 deletion of 36,843 bp nucleotides spanning from the first intron to the last intron of *Dnajb6*
210 gene located in the Chromosome 5, which was created by the insertion of the Velocigene
211 ZEN-Ub1 cassette and subsequent LoxP excision using Cre (Figure 3A). Genotyping PCR
212 using a combination of the *Dnajb6* gene-specific and the Zen-Ubi cassette-specific primers
213 was carried out to identify both Dnajb6 heterozygous (*Dnajb6*$^{+/-}$) and homozygous (*Dnajb6*$^{-/-}$)
214 KO mice (Figure 3B). At the protein level, both the Dnajb6 short (S) and long (L) isoforms
215 were reduced by ~ 50% in *Dnajb6*$^{+/-}$ mouse hearts (Figure 3C), and near completely
216 depleted in *Dnajb6*$^{-/-}$ mutant hearts. Consistent with a previous report,[35] *Dnajb6*$^{-/-}$ KO mice
217 were embryonic lethal, likely due to the placental defects (data not shown). The *Dnajb6*$^{+/-}$
218 mice were able to grow to adulthood without visually noticeable phenotypes until at least 1

219 year of age. Cardiac mechanical function remained normal, as indicated by indistinguishable
220 cardiac echocardiography indices from those of WT siblings at the same age (Table 3).
221 However, significantly increased frequency of SA and AVB episodes, as well as bradycardia
222 phenotype, were noted in the *Dnajb6*$^{+/-}$ mice at 6 months old (Figure 3D and 3E, and Table
223 4). Similar to the *GBT411/dnajb6b* mutant in zebrafish, *Dnajb6*$^{+/-}$ mice exhibited an impaired
224 response to autonomic stimuli including isoproterenol and carbachol (Figure 3E). Together,
225 these studies suggest that *Dnajb6*$^{+/-}$ mice manifest SSS phenotype without
226 structural/functional remodeling of the heart.

227 **2.5 *Ex vivo* evidences of SAN dysfunction in the *Dnajb6*$^{+/-}$ mice**

228 To prove SAN dysfunction in *Dnajb6*$^{+/-}$ mice, we performed electrophysiological assessment
229 of SAN pacemaker function by high-resolution fluorescent optical mapping of action
230 potentials from isolated mouse atria at 1 year of age. We firstly analyzed the distribution of
231 the leading pacemaker location site in *Dnajb6*$^{+/-}$ mice compared to WT control. In WT mice,
232 leading pacemakers were mostly located within the anatomically and functionally defined
233 SAN region (Figure 4A and 4B).[18, 36-38] In contrast, significant increase in the number of
234 leading pacemakers located outside of the SAN, including the subsidiary atrial pacemakers
235 and inter-atrial septum pacemakers, was observed in *Dnajb6*$^{+/-}$ mice. In addition, in *Dnajb6*$^{+/-}$
236 mice, we also found a highly irregular heart rate, accompanied by the presence of multiple
237 competing pacemakers and a beat-to-beat migration of the leading pacemaker between
238 various sites which included SAN, right atrial ectopic (subsidiary) pacemakers, and inter-
239 atrial septum (Figure 4C and 4D). Similar to the results from the *in vivo* studies, bradycardia

phenotype was consistently detected in the isolated atrial preparations as well (Figure 4E). Optical mapping on isolated atrial preparations further revealed different responses of heart rate during isoproterenol, atropine, and carbachol stimulations in *Dnajb6*$^{+/-}$ mice. Significantly increased cycle length (CL) variations were also observed at baseline and upon carbachol stimulation (Figure 4F).

Importantly, in *Dnajb6*$^{+/-}$ mice, we found significant prolongation of the SAN recovery time corrected to beating rate (cSANRT) measured both at baseline and under autonomic stresses, including stimulation by isoproterenol, carbachol, and atropine (Figure 5), confirming the presence of SAN dysfunction in *Dnajb6*$^{+/-}$ mice. Optical mapping also showed that, unlike WT, the first spontaneous post-pacing atrial beats during SANRT measurements in *Dnajb6*$^{+/-}$ mice were originated from ectopic locations outside of the SAN (Figure 5A-B), further supporting a suppressed SAN function.

2.6 Transcriptome analysis of the *Dnajb6*$^{+/-}$ mutant hearts identifies altered genes encoding ion channels and proteins in the Wnt/beta-catenin pathway

To seek molecular mechanisms underlying the SSS phenotypes observed in *Dnajb6*$^{+/-}$ mice, we performed whole transcriptome RNA-sequencing experiments using right atrial tissues isolated from *Dnajb6*$^{+/-}$ and WT mice at 1 year of age. Transcriptomes of biological replicates for *Dnajb6*$^{+/-}$ mice did form a cluster that differs from the cluster for WT control samples, as indicated by principal component analysis (PCA) (Supplemental Figure 3A). Based on a cut-off of adjusted *P* value<0.05, 107 differentially expressed (DE) genes were identified, among which 37 genes were upregulated and 70 genes were downregulated in the *Dnajb6*$^{+/-}$

mutants compared with WT controls (Supplemental Figure 3B and 3C). Through Ingenuity pathway analysis (IPA), several diverse signaling pathways were identified to be altered in the *Dnajb6*$^{+/-}$ mice (Supplemental Figure 3D). Among these 107 differentially expressed genes, we noted calcium handling related protein-encoding genes like *Slc24a2 and Cdh20*, ion channel-encoding genes including *Slc9a3r1, Kcnh7, Fxyd5 and Gjb5* (Figure 6A), as well as 4 Wnt pathway related genes (Figure 6B). We then performed quantitative RT-PCR analysis and experimentally confirmed dysregulation of these genes in the *Dnajb6*$^{+/-}$ mice (Figure 6C). The data on calcium handling and ion channel-encoding genes are in line with the SAN dysfunction phenotype observed in the *Dnajb6*$^{+/-}$ mice. Because Wnt signaling has been shown to direct pacemaker cell specification during SAN morphogenesis,[39, 40] the identification of 4 Wnt pathway related genes could also support the observed SAN dysfunction phenotype in the *Dnajb6*$^{+/-}$ mice.

3. Discussion

3.1 GBT lines enable a phenotype-based screening approach for discovering new SSS genes

This work is based on recent establishment of a GBT protein trap-based insertional mutagenesis screening strategy and the generation of a collection of 1,200 zebrafish mutant strains.[24] Here, we demonstrated the feasibility of screening these GBT lines for discovering new genetic factors for SSS, an aging-associated human disease. To overcome the challenge of colony management efforts that is associated with an adult screen, we leveraged the following unique advantages of the GBT vectors and zebrafish models. First, the knockdown efficiency for the tagged gene in each GBT homozygous mutant is consistently high, which is typically >99%, which ensued the success of an adult screen. Second, because of a fluorescence tag, heterozygous GBT fish can be easily identified under a fluorescent microscope without the need of genotyping. As a consequence, a cardiac expression-based enrichment strategy can be used to identify ZIC lines. Instead of screening 609 GBT lines, only 35 ZIC lines need to be screened, which significantly reduced the workload. We acknowledge that some genes with extremely weak cardiac expression might be missed; however, this is not a concern during the early phase of a genome-wide screen. Third, it is economically feasible to house hundreds of mutant fish lines with different genetic lesions to 1-3 years old. Finally, we optimized an ECG technology, defined the baseline SSS in WT fish, and implemented heat-stress to zebrafish at old ages, which shall increase the SSS phenotypic expressivity.

While the forward genetic screening approach has been successfully utilized to pinpoint genetic basis of cardiogenesis in embryonic fish and doxorubicin-induced cardiomyopathy (DIC) in adult zebrafish,[21, 26] this study extended this powerful genetic approach to adult zebrafish for discovering genetic factors associated with rhythm disorders. Given very little knowledge of molecular underpinnings of SSS, the development of this novel approach is significant. Human genetics approach has been difficult, partially owing to the aging associated nature - SSS-like phenotypes at its early stage are often missed, because SA episodes cannot be detected if the ECG measurement only covers a short time window. It takes years in patients to develop from asymptotic to onset of SSS symptoms. Moreover, human genetic studies of SSS are typically confounded by complicated environmental factors, which are minimalized in our zebrafish forward genetic approach - each ZIC mutant is maintained in a well-controlled living environment, and the only difference among different ZIC lines is a single genetic deficiency.

3.2 *Dnajb6* is a new SSS gene with a unique expression in SAN

The human *DNAJB6* gene encodes a molecular chaperone protein of the heat shock protein 40 (Hsp40) family. Dnajb6 has been previously linked to neurodegenerative diseases via its function in protein folding and the clearance of polyglutamine stretches (polyQ),[41, 42] and to muscular dystrophy via its protein-protein interaction with Bag3 in the sarcomere.[43] Our previous forward genetic screen in adult zebrafish identified *GBT411/dnajb6b* as a deleterious modifier for DIC.[26] Here, we provided several evidences in both fish and mouse models, suggesting new functions of *Dnajb6* as a genetic factor for arrhythmia/SSS. First,

315 *GBT411/dnajb6b* is one of three ZIC lines with SSS-like phenotypes that were identified from
316 a screen of 607 GBT lines that is independent of the previous DIC screen. Second, in
317 zebrafish, the increased incidence of SA episodes and reduced heart rate, two main features
318 of SSS, were detected in 10 monthold *GBT411/dnajb6b* homozygous fish, when structural
319 remodeling/cardiac dysfunction have not yet occurred.[25] Similarly, bradycardia and SA
320 episodes were noted in *Dnajb6*$^{+/-}$ heterozygous KO mice at 6 months old, when the
321 echocardiography indices remained indistinguishable from their age-matched siblings. Third,
322 consistent with loss-of-function studies, Dnajb6 expression was detected in the SAN of both
323 zebrafish and mice. Importantly, Dnajb6 is highly enriched in the SAN region of the mouse
324 comparing to the surrounding atrial tissue. Fourth, transcriptome analysis of *Dnajb6*$^{+/-}$ mice
325 uncovered altered expression of genes involved in calcium handing, ion channels, and Wnt
326 signaling pathway, which have been linked to the formation/function of the SAN. Together,
327 we conclude that SSS might not be a consequence of Dnajb6 cardiomyopathy. Instead, the
328 irregular heartbeat is most likely a direct consequence of Dnajb6 depletion in pacemaker
329 cells, subsequently contributing to the pathogenesis of cardiomyopathy that occurs later. To
330 ultimately confirm this hypothesis and to discern functions of Dnajb6 in SAN pacemakers
331 from working cardiomyocytes, a tissue-specific KO line for Dnajb6 needs to be generated
332 and studied.

333 Detailed examination of Dnajb6 expression in the SAN uncovered unique expression
334 patterns. While Dnajb6 is highly expressed in the SAN and overlaps with one of the main
335 SAN progenitors ISL1 (Figure 2C and 2F), we found a poor co-expression with one of the

main pacemaker protein HCN4: Dnajb6-positive cells overlap only with a small portion of the HCN4-positive cells (Figure 2C and 2D). This is supported by a negative correlation between the expression level of Dnajb6 and Tbx3, as Tbx3 is one of the main transcriptional regulators of HCN4 expression in cardiac conduction system.[44, 45] While these results may sound surprising, studies on isolated SAN cells reported dramatic variability in the density of HCN-formed "funny" current I_f.[46-49] In spontaneously beating cardiomyocytes isolated from the rabbit SAN, Monfredi et al. showed that I_f density can range from 0 to ~50 pA/pF and some the spontaneously beating SAN cells may have little to zero I_f.[48] The authors further observed SAN cells with lower I_f current densities demonstrated a significantly greater sensitivity to inhibition of Ca^{2+} clock component of the SAN pacemaking machinery by cyclopiazonic acid, a moderate disruptor of Ca^{2+} cycling, in terms of beating rate slowing. The authors also noted that a relatively large cell population (21 of 90 cells) stopped beating when the sarcoplasmic reticulum pumping rate decreased in the presence of CPA, despite a relatively high I_f density. Together with other studies,[33, 50] these results may indicate a significant functional heterogeneity of pacemaker cells within the SAN in terms of their spontaneous beating rate, ion channel and calcium handling protein expression repertoire, and molecular mechanisms of their pacemaker activities. The latter was recently linked to the balance between the voltage and calcium components of the coupled-clock pacemaker system describing mechanisms of SAN automaticity.[51] As summarized in details in our recent review,[52] it was suggested that pacemaker cells, which primary rely on the Ca^{2+} clock, are more sensitive to the autonomic modulation through cAMP-mediated regulation of

phosphorylation of Ca^{2+} handling proteins.[50] This is in line with our findings indicating that Dnajb6 is mainly expressed in SAN cells with low HCN4 density (Figure 2D) and that Dnajb6 knock-out affects calcium homeostasis genes (Figure 6) and leads to abnormal autonomic regulation of the SAN (Figure 3E and Figure 4). Though our studies strongly support a crucial role of Dnajb6 in SAN automaticity and autonomic regulation of SAN pacemaking, detailed studies are needed to determine exact cellular and molecular pathways involved in these mechanisms.

3.3 A phenotype-based screening approach would facilitate the elucidation of molecular basis of SSS

Besides *dnajb6b*, our pilot forward genetic screen also suggested two additional candidate SSS genes like *cyth3a* and *vapal*, pending more experimental evidence to confirm their function. This forward genetic screening approach is scalable to the genome, which would generate a comprehensive list of candidate genes for SSS. Because there are at least 3 major cell types in the SAN region, including pacemaker cells in SAN that generate rhythm, paranodal areas and transition cells in the atrium that transmit the signal from pacemaker cells to govern coordinated contraction of the heart from atrium and then to the ventricle,[53, 54] newly identified SSS genes could be categorized into different groups based on their expression pattern and phenotypic traits. We anticipate that systematic studies of these candidate genes identified from zebrafish will significantly advance our understanding of pathophysiology of SSS.

4. Materials and methods

4.1 Animals

All experiments were conducted in accordance with the National Institutes of Health Guide for the Care and Use of Laboratory Animals (NIH Pub. No. 80-23). All methods and protocols used in these studies have been approved by the Mayo Clinic Institutional Animal Care and Use Committee and by the Animal Care and Use Committee of University of Wisconsin-Madison, following the Guidelines for the Care and Use of Laboratory Animals published by the US National Institutes of Health (publication No. 85-23, revised 1996). The zebrafish (*Danio rerio*) WIK line was maintained under a 14-hour light/10-hour dark cycle at 28.5°C. All GBT lines were generated previously.[23-25] The *Dnajb6* knockout (KO) mice, originally named *Dnajb6*$^{tm1.1(KOMP)Vlcg}$, were generated from the Jackson Laboratory (Original catalog #018623). Briefly, the insertion of Velocigene cassette ZEN-Ub1 created a deletion sized 36,843 bp nucleotides spanning from the first to the last intron of the *Dnajb6* gene at the Chromosome 5 (Genome Build37) of the C57BL/6N mice. The mouse was subsequently bred to a ubiquitous Cre deletion mouse line for recombination of the LoxP sites that excised the neomycin selection cassette. The following genotyping PCR primers for the *Dnajb6* mutant mice were used: mutant primer F2, 5'-AAACTGCGCACTGTACCACC-3' and mutant primer R2, 5'-CGGTCGCTACCATTACCAGT-3' for detecting the mutant allele (predicted size of 700 bp); and WT primer F1, 5'-TACTCCAGCCCCACTCTTACTC-3' and WT primer R1, 5'-ACTGCCCATCTTCTTCAACTTC-3' for detecting the WT allele (predicted size of 300 bp).

4.2 Enrichment and cloning of 35 ZIC mutants

Zebrafish cardiac insertional (ZIC) mutants were identified and collected based on the mRFP expression in the embryonic heart from 2 to 4 days post-fertilization (dpf) and/or in the dissected adult heart at 6 months to 1 year of age. All ZIC lines, each with a single copy of GBT insertion, were obtained after 2 to 4 generations of outcrosses, guided by Southern blotting using the *GFP* probe primed to the GBT vector.[25] A combination of 3 different methods including Inverse PCR, 5'-RACE and/or 3'-RACE were employed to clone the GBT transposon integration sites accordingly to previously published protocols.[23-25]

4.3 Zebrafish Electrocardiogram (ECG)

Microsurgery was operated under a dissection microscope to remove the silvery epithelial layer of the hypodermis one week before fish were subjected to the ECG.[29] Fish were initially acclimated for one hour after transferred from the circulating fish facility to the laboratory bench, followed by anesthesia in the solution of pH 7.0 adjusted tricaine (MS-222, Sigma) at the concentration of 0.02% dissolved in E3 medium (containing 5 mM NaCl, 0.17 mM KCl, 0.33 mM $CaCl_2$, and 0.33 mM $MgSO_4$) for 6 minutes. Two minutes of ECG recording were then obtained with the ECG recording system, according to the instructions (ZS-200, iWorx Systems, Inc) and a recently published protocol.[29] Initial ECG screens of ZIC heterozygous mutants were performed at 32°C using a temperature-controlled chamber set-up, made by covering the ECG recording system with a foam box. 6 to 25 fish per ZIC line were initially analyzed, depending on the fish availability. The ECG machine was held on top of a heating plate controlled by a heating machine. The subsequent ECG validation in the homozygous mutants was performed at room temperature (25°C). To analyze the ECG recording, ECG

signals were amplified and filtered at 0.5 Hz high pass and 200 Hz low pass. ECG variables, including heart rate, P-wave amplitude, R-wave amplitude, and PP and RR intervals were calculated using an in-house Matlab code.[55] A SA episode was defined in zebrafish when the PP interval is more than 1.5 seconds.

4.4 Mouse ECG and echocardiography

Mouse echocardiography and ECG measurements were performed according to a previously published protocol with modifications.[26, 27] For ECG, mice were anesthetized with isoflurane (0.5% to 1.0% v/v) via a nose cone. Mice were placed on an ECG-heater board with 4 paws on individual electrodes. The ECG-heater board maintained the body temperature at 37°C. The ECG signal was amplified through an amplifier (Axon CNS digital 1440 A) and recorded using Chart 5 software. For each mouse, 10 min of ECG signal were recorded. Series of ECG parameters, including heart rate, P-wave amplitude, R-wave amplitude, PP/RR interval were calculated by an in-house Matlab code.[55] For echocardiography, mice were anesthetized under light isoflurane (0.5% to 1.0% v/v) administered via a nose cone. Echocardiography gel was placed on the shaved chest, and the mouse heart was imaged with a 13-MHz probe using 2-dimensional echocardiography (GE Healthcare). All measurements were made by an independent operator to whom the study groups were masked.

4.5 Administration of autonomic response drugs

For zebrafish, 0.6 μg/g isoproterenol (Millipore Sigma, Cat# 1351005), 4 μg/g atropine (Millipore Sigma, Cat# A0132), and 0.3 μg/g carbachol (Millipore Sigma, cat# C4382) were

administrated via intraperitoneal injection. For *in vivo* mouse studies, 0.2 mg/kg isoproterenol, 1 mg/kg atropine, and 0.3 mg/kg carbachol was injected intraperitoneally. For *ex vivo* mouse atrial studies, 100 nM isoproterenol, 2 μM atropine, and 300 nM carbachol was administered via superfusion for 10 - 20 min.

4.6 Antibody immunostaining

Heart samples harvested from mouse SAN tissues were embedded in a tissue freezing medium, followed by sectioning at 10 μm using a cryostat (Leica CM3050 S). The slides were subjected to immunostaining using a previously described protocol.[56] The following antibodies were used: anti-HCN4 (Millipore, Cat#: AB5805) at 1:200, anti-Dnajb6 (Novus, Cat#: H00010049-M01) at 1:200, anti-Islet1 (abcam, Cat#: ab20670), anti-Tbx3 (abcam, Cat#: ab99302). All images were captured either using a Zeiss Axioplan II microscope equipped with ApoTome and AxioVision software (Carl Zeiss Microscopy) or a Zeiss LSM 780 confocal microscope.

4.7 Isolated mouse atrial preparations

The mouse atrial preparation was performed as previously described.[57] After the mice were anesthetized with isoflurane, a mid-sternal incision was applied. The heart was then removed and cannulated to a custom made 21-gauge cannula. The heart was then perfused and superfused with oxygenated (95% O_2, 5% CO_2), 37°C modified Tyrode solution (in mM: 128.2 NaCl, 4.7 KCl, 1.19 NaH_2PO_4, 1.05 $MgCl_2$, 1.3 $CaCl_2$, 20.0 $NaHCO_3$, and 11.1 glucose; pH=7.35±0.05). Lung, thymus and fat tissue was then removed. Perfusion was maintained under constant aortic pressure of 60-80 mmHg. After 10 min stabilization, the

ventricles were dissected. The atrial were cut open as previously described.[58] The medial limb of the crista terminalis was cut to open right atrial appendage. The preparation was superfused with Tyrode solution at a constant rate of ~ 15 ml/min.

4.8 Optical mapping

High spatial (100x100 pixels, 60 ± 10μm per pixel) and temporal (1,000 – 3,000 frames/sec) resolution optical mapping of electrical activity was applied on the isolated mouse atrial preparations as previously described.[58, 59] The isolated mouse atrial preparations were coronary and surface stained with voltage-sensitive dye RH-237 (1.25 mg/ml in dimethyl sulfoxide ThermoFisher Scientific, USA). Blebbistatin (10 μM, Tocris Bioscience, USA) was then applied to reduce the motion artifact. A 150-W halogen lamp (MHAB-150W, Moritex USA Inc., CA, USA) with band pass filter (530/40 nm) was used as excitation light source. The fluorescent light emitted from the preparation was recorded by a MiCAM Ultima-L camera (SciMedia, CA, USA) after a long-pass filter (>650 nm). The acquired fluorescent signal was digitized, amplified, and visualized using custom software (SciMedia, CA, USA). After 20-30 min stabilization, activation map was collected during baseline spontaneous rhythm. To estimate the pacemaker location and a possible pacemaker shift during autonomic stimulation, the originations of action potentials were plotted with orthogonal axes crossing at the inferior vena cava. The superior to inferior direction is along the ordinate. The lateral to media direction is along the abscissa. SAN recovery time (SANRT) was measured as the time-period between the last S1S1 pacing (10 Hz) beat and the first spontaneous beat. Corrected SANRT (SANRTc) was calculated as the difference between the SANRT

and the resting cycle length measure before the SANRT pacing protocol. After baseline measurement, 100 nM isoproterenol was applied. Recordings were collected after 10 min which allows the stimulation to reach steady-state effect. Complete washout was then performed which is characterized by the recovery of the heart rate back to baseline values. Additional staining and blebbistatin was applied as needed. 300 nM carbachol then was applied. 2 μM atropine was used after protocols completed during carbachol stimulation.

4.9 RNA-seq data collection and analysis

Total RNA was extracted from the right atrium (RA) tissues of 1-year-old *Dnajb6*$^{+/-}$ heterozygous mutant hearts and WT sibling controls. Six total samples (3 biological replicates for each genotype) were submitted for RNA sequencing (Azenta Life Science, NJ). Genes were considered to be differentially expressed between the two groups if they exhibited a greater than 2-fold change and an FDR of less than 0.05 according to the DESeq approach.[61] Unsupervised hierarchical clustering was performed with Pearson correlation and scaled based on the fragments per kilobase of transcript per million mapped reads (FPKM) value using the pheatmap R package (https://github.com/raivokolde/pheatmap). The gene lists of interest were annotated by IPA (QIAGEN) (http://www.ingenuity.com/). We queried the IPA with the gene list of interest to map and generate putative biological processes/functions, networks, and pathways based on the manually curated knowledge database of molecular interactions extracted from the public literature. The enriched pathways and gene networks were generated using both direct and indirect

relationships/connectivity. These pathways and networks were ranked by their enrichment score, which measures the probability that the genes were included in a network by chance.

4.10 Quantitative reverse transcription (RT) PCR

Total RNA was extracted from ~2 mg of right atrium (RA) tissues of 1-year-old *Dnajb6*$^{+/-}$ heterozygous mutant hearts and WT sibling controls using Trizol reagent (ThermoFisher Scientific) following the manufacturer's instruction. Approximately 1 μg total RNA was used for reverse transcription (RT) and cDNA synthesis using Superscript III First-Strand Synthesis System (ThermoFisher Scientific). Real-time quantitative RT-PCR was run in 96-well optical plates (ThermoFisher Scientific) using an Applied Biosystem VAii 7 System (ThermoFisher Scientific). Gene expression levels were normalized using the expression level of glyceraldehyde 3-phosphate dehydrogenase (*gapdh)* by –ΔΔCt (cycle threshold) values. All quantitative RT-PCR primer sequences were listed in Supplemental Table 2.

4.10 Statistics

No sample sizes were calculated before performing the experiments. No animals were excluded for analysis. Unpaired 2-tailed student's *t*-test was used to compare 2 groups. One-way Analysis of Variance (ANOVA) or Kruskal-Wallis test followed by post hoc Tukey's test was used for comparing 3 and more groups. Chi-square test was used for rate comparison. *P* values less than 0.05 was considered statistically significant. For dot plot graphs, values are displayed as mean ± standard deviation (SD). Sample size (N) represents animal number, otherwise specifically designated as biological or technical replicates. All statistical

analyses were conducted with the Graphpad Prism 7 and/or R Statistical Software Version 3.6.1.

Acknowledgments

We thank Beninio Gores and Kashia Stragey for managing zebrafish facility and Ronald H. May for murine echocardiography.

Sources of Funding

This work was supported in part by grants from the Mayo Foundation to X.X., Grants from YG Li (Science and Technology Innovation Action Plan of Shanghai, experimental animal research project 201409005600), NIH R01HL141214, American Heart Association 16SDG29120011, and the Wisconsin Partnership Program 4140 to A.V.G., and American Heart Association 17POST33370089 and American Heart Association Career Development Award 846898 to D. L.

Figure Legends

Figure 1. Screening of 35 ZIC lines identified 3 mutants with increased incidence of SA and/or AVB episodes

(A) Representative ECG recordings for 3 heterozygous GBT mutants with incidence of sinus arrest (SA) and/or atrioventricular block (AVB) episodes compared to WT control. **(B)** RP2 gene-break transposon insertional positions in the 3 candidate SSS mutants.

Figure 2. Dnajb6 is expressed in the SAN in both zebrafish and mouse

(A-B) Co-localization analysis of mRFP in *GBT411/dnajb6b* with the reporter line sqET33-mi59B in which EGFP labels cardiac conduction system (CCS) in zebrafish. The mRFP reporter for the *GBT411* tagged Dnajb6b protein partially overlaps with the EGFP reporter in the sqET33-mi59B transgenic line that labels the SAN in embryonic atrium at 3 dpf (A) and atrio-ventricular canal (AVC) in adult hearts (B). Arrows indicate EGFP+ cells in the sqET33-mi59B reporter line. A: atrium. V: ventricle. dpf, days post-fertilization. **(C)** The Dnajb6 antibody immunostaining signal largely overlapped with the HCN4 immunostaining signal in mouse SAN tissues under low magnification. **(D)** Under higher magnification, expression of Dnajb6 (red) only partially overlapped with HCN4 (green) as revealed by antibody co-immunostaining. Arrows point to cells with overlapping patterns. Arrowheads point to cells with no-overlapping. **(E)** Shown are images indicating expression of Dnajb6 protein largely overlapping with the Tbx3 antibody immunostaining with medium to low intensity, but not strong signal in the SAN tissues. Arrows point to cells with strong Tbx3 immunostaining signal. Arrowheads point to cells with medium to low level of Tbx3 immunostaining signal.

(F) Shown are images indicating expression of Dnajb6 protein largely overlapping with the Islet1, a transcription factor labeling SAN cells. Arrows point to cells with overlapping immunostaining signal for both Dnajb6 and Islet1. Scale bars in A, C, 50 μm. Scale bars in B, D, E, F, 20 μm.

Figure 3. *Dnajb6*$^{+/-}$ mice exhibited increased incidence of SA and AVB and impaired response to autonomic stimuli

(A) Schematics of the Dnajb6 knockout (KO) mice. The insertion of Velocigene cassette ZEN-Ub1 created a deletion of 36,843 bp nucleotides spanning from the first to the last intron of the *Dnajb6* gene at the Chromosome 5. The neomycin selection cassette was excised after crossed to a Cre expression line. **(B)** Representative DNA gel images of PCR genotyping for identifying WT (300 bp), *Dnajb6*$^{+/-}$ heterozygous (hets), and *Dnajb6*$^{-/-}$ homozygous (homo) mutant alleles (700 bp). **(C)** Western blotting and quantification of Dnajb6 short (S) and long (L) protein expression in WT and *Dnajb6* mutants. N=3 animal per group. **(D)** Shown are representative ECG recordings results showing SA and AVB phenotypes detected in the *Dnajb6*$^{+/-}$ mice at 6 months. **(E)** The *Dnajb6*$^{+/-}$ mice manifests impaired response to different autonomic stimuli. N=10-12 mice per group. Unpaired student's *t*-test. SA, sinus arrest. AVB, atrioventricular block.

Figure 4. SAN dysfunction in the *Dnajb6*$^{+/-}$ mice

(A) Leading pacemakers were located and plotted from both WT (blue dots) and *Dnajb6*$^{+/-}$ (red dots) mice. One mouse could have multiple leading pacemaker locations due to the competing pacemakers and ectopic activities. SVC and IVC, superior and inferior vena cava;

RAA, right atrial appendage; CT, crista terminalis; IAS, inter-atrial septum; AVN, atrioventricular node. Distribution of the leading pacemakers is summarized in panel. **(B)** Majority of leading pacemakers located within the SAN area in WT whereas, in *Dnajb6*$^{+/-}$ mice, significant increase of leading pacemakers locating in subsidiary pacemaker area and IAS was observed. **(C-D)** Activation map based on the optical mapping of action potentials showed representative leading pacemaker locations in WT (SAN) and *Dnajb6*$^{+/-}$ mice (SAN and IAS areas). **(E)** Optical mapping on isolated atrial preparation showed bradycardia (baseline) and different responses of heart rate during isoproterenol, atropine, and carbachol stimulations between WT and *Dnajb6*$^{+/-}$ mice. N=7-9 mice per group. Unpaired student's *t*-test. **(F)** Increased cycle length (CL) variation was observed in *Dnajb6*$^{+/-}$ isolated atrial preparations during different autonomic stimulations. N=7-9 mice per group. Unpaired student's *t*-test.

Figure 5. Sinus node recovery time was prolonged in the *Dnajb6*$^{+/-}$ mice

(A-B) Representative activation maps reconstructed for the last pacing stimulus (S1) and the first spontaneous post-pacing atrial beat (A1) during SAN recovery time (SANRT) measurements are shown. A site of the earliest atrial activation is labeled by a white asterisk. In *Dnajb6*$^{+/-}$ group, unlike WT, the first spontaneous post-pacing atrial beat (A1) originated from an ectopic location outside of the anatomically and functionally defined SAN area. **(C)** Summarized data for corrected SANRT (SANRTc) measured during different autonomic stimulations is shown. N=7-9 mice per group. Unpaired student's *t*-test.

Figure 6. Transcriptomes are altered in the atrium of *Dnajb6*$^{+/-}$ mice

(A) Expression of six calcium homeostasis and ion channel related genes were altered in the *Dnajb6*$^{+/-}$ mice atrium. **(B)** Expression of four Wnt pathway related genes were altered in the *Dnajb6*$^{+/-}$ mice atrium. **(C)** Quantitative polymerase chain reaction (qPCR) validation of DE genes listed in A and B, normalized to Gapdh; RNA was extracted from an individual moue atrium, which was considered a single biological replicate. Samples were collected in triplicate. N=3 mice per group. Unpaired student's *t*-test.

References

1. Khurshid S, Choi SH, Weng LC, Wang EY, Trinquart L, Benjamin EJ, Ellinor PT and Lubitz SA. Frequency of Cardiac Rhythm Abnormalities in a Half Million Adults. *Circ Arrhythm Electrophysiol*. 2018;11:e006273.
2. Semelka M, Gera J and Usman S. Sick sinus syndrome: a review. *Am Fam Physician*. 2013;87:691-6.
3. De Ponti R, Marazzato J, Bagliani G, Leonelli FM and Padeletti L. Sick Sinus Syndrome. *Card Electrophysiol Clin*. 2018;10:183-195.
4. Dakkak W and Doukky R. Sick Sinus Syndrome *StatPearls* Treasure Island (FL); 2020.
5. Mond HG and Proclemer A. The 11th world survey of cardiac pacing and implantable cardioverter-defibrillators: calendar year 2009--a World Society of Arrhythmia's project. *Pacing Clin Electrophysiol*. 2011;34:1013-27.
6. Nof E, Luria D, Brass D, Marek D, Lahat H, Reznik-Wolf H, Pras E, Dascal N, Eldar M and Glikson M. Point mutation in the HCN4 cardiac ion channel pore affecting synthesis, trafficking, and functional expression is associated with familial asymptomatic sinus bradycardia. *Circulation*. 2007;116:463-70.
7. Tan HL, Bink-Boelkens MT, Bezzina CR, Viswanathan PC, Beaufort-Krol GC, van Tintelen PJ, van den Berg MP, Wilde AA and Balser JR. A sodium-channel mutation causes isolated cardiac conduction disease. *Nature*. 2001;409:1043-7.
8. Schulze-Bahr E, Neu A, Friederich P, Kaupp UB, Breithardt G, Pongs O and Isbrandt D. Pacemaker channel dysfunction in a patient with sinus node disease. *J Clin Invest*. 2003;111:1537-45.
9. Verkerk AO and Wilders R. Pacemaker activity of the human sinoatrial node: an update on the effects of mutations in HCN4 on the hyperpolarization-activated current. *Int J Mol Sci*. 2015;16:3071-94.
10. Anderson JB and Benson DW. Genetics of Sick Sinus Syndrome. *Card Electrophysiol Clin*. 2010;2:499-507.
11. Holm H, Gudbjartsson DF, Sulem P, Masson G, Helgadottir HT, Zanon C, Magnusson OT, Helgason A, Saemundsdottir J, Gylfason A, Stefansdottir H, Gretarsdottir S, Matthiasson SE, Thorgeirsson GM, Jonasdottir A, Sigurdsson A, Stefansson H, Werge T, Rafnar T, Kiemeney LA, Parvez B, Muhammad R, Roden DM, Darbar D, Thorleifsson G, Walters GB, Kong A, Thorsteinsdottir U, Arnar DO and Stefansson K. A rare variant in MYH6 is associated with high risk of sick sinus syndrome. *Nat Genet*. 2011;43:316-20.
12. Zhu YB, Luo JW, Jiang F and Liu G. Genetic analysis of sick sinus syndrome in a family harboring compound CACNA1C and TTN mutations. *Mol Med Rep*. 2018;17:7073-7080.
13. Monfredi O and Boyett MR. Sick sinus syndrome and atrial fibrillation in older persons - A view from the sinoatrial nodal myocyte. *J Mol Cell Cardiol*. 2015;83:88-100.
14. Lin J and Musunuru K. From Genotype to Phenotype: A Primer on the Functional Follow-up of Genome-Wide Association Studies in Cardiovascular Disease. *Circ Genom Precis Med*. 2018;11.
15. Tam V, Patel N, Turcotte M, Bosse Y, Pare G and Meyre D. Benefits and limitations of genome-wide association studies. *Nat Rev Genet*. 2019;20:467-484.
16. Kamp A, Peterson MA, Svenson KL, Bjork BC, Hentges KE, Rajapaksha TW, Moran J, Justice MJ, Seidman JG, Seidman CE, Moskowitz IP and Beier DR. Genome-wide identification of mouse congenital heart disease loci. *Hum Mol Genet*. 2010;19:3105-13.
17. Shen Y, Leatherbury L, Rosenthal J, Yu Q, Pappas MA, Wessels A, Lucas J, Siegfried B, Chatterjee B, Svenson K and Lo CW. Cardiovascular phenotyping of fetal mice by noninvasive high-frequency ultrasound

facilitates recovery of ENU-induced mutations causing congenital cardiac and extracardiac defects. *Physiol Genomics*. 2005;24:23-36.
18. Gut P, Reischauer S, Stainier DYR and Arnaout R. Little Fish, Big Data: Zebrafish as a Model for Cardiovascular and Metabolic Disease. *Physiol Rev*. 2017;97:889-938.
19. Bakkers J. Zebrafish as a model to study cardiac development and human cardiac disease. *Cardiovasc Res*. 2011;91:279-88.
20. Ding Y, Bu H and Xu X. Modeling Inherited Cardiomyopathies in Adult Zebrafish for Precision Medicine. *Front Physiol*. 2020;11:599244.
21. Amsterdam A, Burgess S, Golling G, Chen W, Sun Z, Townsend K, Farrington S, Haldi M and Hopkins N. A large-scale insertional mutagenesis screen in zebrafish. *Genes Dev*. 1999;13:2713-24.
22. Wang D, Jao LE, Zheng N, Dolan K, Ivey J, Zonies S, Wu X, Wu K, Yang H, Meng Q, Zhu Z, Zhang B, Lin S and Burgess SM. Efficient genome-wide mutagenesis of zebrafish genes by retroviral insertions. *Proc Natl Acad Sci U S A*. 2007;104:12428-33.
23. Clark KJ, Balciunas D, Pogoda HM, Ding Y, Westcot SE, Bedell VM, Greenwood TM, Urban MD, Skuster KJ, Petzold AM, Ni J, Nielsen AL, Patowary A, Scaria V, Sivasubbu S, Xu X, Hammerschmidt M and Ekker SC. In vivo protein trapping produces a functional expression codex of the vertebrate proteome. *Nat Methods*. 2011;8:506-15.
24. Ichino N, Serres MR, Urban RM, Urban MD, Treichel AJ, Schaefbauer KJ, Greif LE, Varshney GK, Skuster KJ, McNulty MS, Daby CL, Wang Y, Liao HK, El-Rass S, Ding Y, Liu W, Anderson JL, Wishman MD, Sabharwal A, Schimmenti LA, Sivasubbu S, Balciunas D, Hammerschmidt M, Farber SA, Wen XY, Xu X, McGrail M, Essner JJ, Burgess SM, Clark KJ and Ekker SC. Building the vertebrate codex using the gene breaking protein trap library. *Elife*. 2020;9.
25. Ding Y, Liu W, Deng Y, Jomok B, Yang J, Huang W, Clark KJ, Zhong TP, Lin X, Ekker SC and Xu X. Trapping cardiac recessive mutants via expression-based insertional mutagenesis screening. *Circ Res*. 2013;112:606-17.
26. Ding Y, Long PA, Bos JM, Shih YH, Ma X, Sundsbak RS, Chen J, Jiang Y, Zhao L, Hu X, Wang J, Shi Y, Ackerman MJ, Lin X, Ekker SC, Redfield MM, Olson TM and Xu X. A modifier screen identifies DNAJB6 as a cardiomyopathy susceptibility gene. *JCI Insight*. 2016;1.
27. Ding Y, Yang J, Chen P, Lu T, Jiao K, Tester DJ, Giudicessi JR, Jiang K, Ackerman MJ, Li Y, Wang DW, Lee HC, Wang DW and Xu X. Knockout of SORBS2 Protein Disrupts the Structural Integrity of Intercalated Disc and Manifests Features of Arrhythmogenic Cardiomyopathy. *J Am Heart Assoc*. 2020;9:e017055.
28. Ma X, Zhu P, Ding Y, Zhang H, Qiu Q, Dvornikov AV, Wang Z, Kim M, Wang Y, Lowerison M, Yu Y, Norton N, Herrmann J, Ekker SC, Hsiai TK, Lin X and Xu X. Retinoid X receptor alpha is a spatiotemporally predominant therapeutic target for anthracycline-induced cardiotoxicity. *Sci Adv*. 2020;6:eaay2939.
29. Yan J, Li H, Bu H, Jiao K, Zhang AX, Le T, Cao H, Li Y, Ding Y and Xu X. Aging-associated sinus arrest and sick sinus syndrome in adult zebrafish. *PLoS One*. 2020;15:e0232457.
30. Poon KL, Liebling M, Kondrychyn I, Brand T and Korzh V. Development of the cardiac conduction system in zebrafish. *Gene Expr Patterns*. 2016;21:89-96.
31. Abu Nahia K, Migdal M, Quinn TA, Poon KL, Lapinski M, Sulej A, Liu J, Mondal SS, Pawlak M, Bugajski L, Piwocka K, Brand T, Kohl P, Korzh V and Winata C. Genomic and physiological analyses of the zebrafish atrioventricular canal reveal molecular building blocks of the secondary pacemaker region. *Cell Mol Life Sci*. 2021;78:6669-6687.

32. Liang X, Zhang Q, Cattaneo P, Zhuang S, Gong X, Spann NJ, Jiang C, Cao X, Zhao X, Zhang X, Bu L, Wang G, Chen HS, Zhuang T, Yan J, Geng P, Luo L, Banerjee I, Chen Y, Glass CK, Zambon AC, Chen J, Sun Y and Evans SM. Transcription factor ISL1 is essential for pacemaker development and function. *J Clin Invest*. 2015;125:3256-68.

33. Boyett MR, Honjo H and Kodama I. The sinoatrial node, a heterogeneous pacemaker structure. *Cardiovasc Res*. 2000;47:658-87.

34. Liang D, Xue J, Geng L, Zhou L, Lv B, Zeng Q, Xiong K, Zhou H, Xie D, Zhang F, Liu J, Liu Y, Li L, Yang J, Xue Z and Chen YH. Cellular and molecular landscape of mammalian sinoatrial node revealed by single-cell RNA sequencing. *Nat Commun*. 2021;12:287.

35. Hunter PJ, Swanson BJ, Haendel MA, Lyons GE and Cross JC. Mrj encodes a DnaJ-related co-chaperone that is essential for murine placental development. *Development*. 1999;126:1247-58.

36. Glukhov AV, Fedorov VV, Anderson ME, Mohler PJ and Efimov IR. Functional anatomy of the murine sinus node: high-resolution optical mapping of ankyrin-B heterozygous mice. *Am J Physiol Heart Circ Physiol*. 2010;299:H482-91.

37. Liu J, Dobrzynski H, Yanni J, Boyett MR and Lei M. Organisation of the mouse sinoatrial node: structure and expression of HCN channels. *Cardiovasc Res*. 2007;73:729-38.

38. Verheijck EE, van Kempen MJ, Veereschild M, Lurvink J, Jongsma HJ and Bouman LN. Electrophysiological features of the mouse sinoatrial node in relation to connexin distribution. *Cardiovasc Res*. 2001;52:40-50.

39. Liang W, Han P, Kim EH, Mak J, Zhang R, Torrente AG, Goldhaber JI, Marban E and Cho HC. Canonical Wnt signaling promotes pacemaker cell specification of cardiac mesodermal cells derived from mouse and human embryonic stem cells. *Stem Cells*. 2020;38:352-368.

40. Ren J, Han P, Ma X, Farah EN, Bloomekatz J, Zeng XI, Zhang R, Swim MM, Witty AD, Knight HG, Deshpande R, Xu W, Yelon D, Chen S and Chi NC. Canonical Wnt5b Signaling Directs Outlying Nkx2.5+ Mesoderm into Pacemaker Cardiomyocytes. *Dev Cell*. 2019;50:729-743 e5.

41. Gillis J, Schipper-Krom S, Juenemann K, Gruber A, Coolen S, van den Nieuwendijk R, van Veen H, Overkleeft H, Goedhart J, Kampinga HH and Reits EA. The DNAJB6 and DNAJB8 protein chaperones prevent intracellular aggregation of polyglutamine peptides. *J Biol Chem*. 2013;288:17225-37.

42. Hageman J, Rujano MA, van Waarde MA, Kakkar V, Dirks RP, Govorukhina N, Oosterveld-Hut HM, Lubsen NH and Kampinga HH. A DNAJB chaperone subfamily with HDAC-dependent activities suppresses toxic protein aggregation. *Mol Cell*. 2010;37:355-69.

43. Sarparanta J, Jonson PH, Golzio C, Sandell S, Luque H, Screen M, McDonald K, Stajich JM, Mahjneh I, Vihola A, Raheem O, Penttila S, Lehtinen S, Huovinen S, Palmio J, Tasca G, Ricci E, Hackman P, Hauser M, Katsanis N and Udd B. Mutations affecting the cytoplasmic functions of the co-chaperone DNAJB6 cause limb-girdle muscular dystrophy. *Nat Genet*. 2012;44:450-5, S1-2.

44. Hoogaars WM, Engel A, Brons JF, Verkerk AO, de Lange FJ, Wong LY, Bakker ML, Clout DE, Wakker V, Barnett P, Ravesloot JH, Moorman AF, Verheijck EE and Christoffels VM. Tbx3 controls the sinoatrial node gene program and imposes pacemaker function on the atria. *Genes Dev*. 2007;21:1098-112.

45. Mohan RA, Bosada FM, van Weerd JH, van Duijvenboden K, Wang J, Mommersteeg MTM, Hooijkaas IB, Wakker V, de Gier-de Vries C, Coronel R, Boink GJJ, Bakkers J, Barnett P, Boukens BJ and Christoffels VM. T-box transcription factor 3 governs a transcriptional program for the function of the mouse atrioventricular conduction system. *Proc Natl Acad Sci U S A*. 2020;117:18617-18626.

730 46. Honjo H, Boyett MR, Kodama I and Toyama J. Correlation between electrical activity and the size of
731 rabbit sino-atrial node cells. *J Physiol*. 1996;496 (Pt 3):795-808.
732 47. Mangoni ME and Nargeot J. Properties of the hyperpolarization-activated current (I(f)) in isolated
733 mouse sino-atrial cells. *Cardiovasc Res*. 2001;52:51-64.
734 48. Monfredi O, Tsutsui K, Ziman B, Stern MD, Lakatta EG and Maltsev VA. Electrophysiological
735 heterogeneity of pacemaker cells in the rabbit intercaval region, including the SA node: insights from recording
736 multiple ion currents in each cell. *Am J Physiol Heart Circ Physiol*. 2018;314:H403-H414.
737 49. Wilders R, Verheijck EE, Kumar R, Goolsby WN, van Ginneken AC, Joyner RW and Jongsma HJ. Model
738 clamp and its application to synchronization of rabbit sinoatrial node cells. *Am J Physiol*. 1996;271:H2168-82.
739 50. Kim MS, Maltsev AV, Monfredi O, Maltseva LA, Wirth A, Florio MC, Tsutsui K, Riordon DR, Parsons SP,
740 Tagirova S, Ziman BD, Stern MD, Lakatta EG and Maltsev VA. Heterogeneity of calcium clock functions in
741 dormant, dysrhythmically and rhythmically firing single pacemaker cells isolated from SA node. *Cell Calcium*.
742 2018;74:168-179.
743 51. Lakatta EG, Maltsev VA and Vinogradova TM. A coupled SYSTEM of intracellular Ca2+ clocks and
744 surface membrane voltage clocks controls the timekeeping mechanism of the heart's pacemaker. *Circ Res*.
745 2010;106:659-73.
746 52. Lang D and Glukhov AV. Cellular and Molecular Mechanisms of Functional Hierarchy of Pacemaker
747 Clusters in the Sinoatrial Node: New Insights into Sick Sinus Syndrome. *J Cardiovasc Dev Dis*. 2021;8.
748 53. Li N, Hansen BJ, Csepe TA, Zhao J, Ignozzi AJ, Sul LV, Zakharkin SO, Kalyanasundaram A, Davis JP,
749 Biesiadecki BJ, Kilic A, Janssen PML, Mohler PJ, Weiss R, Hummel JD and Fedorov VV. Redundant and diverse
750 intranodal pacemakers and conduction pathways protect the human sinoatrial node from failure. *Sci Transl*
751 *Med*. 2017;9.
752 54. Li N, Kalyanasundaram A, Hansen BJ, Artiga EJ, Sharma R, Abudulwahed SH, Helfrich KM, Rozenberg
753 G, Wu PJ, Zakharkin S, Gyorke S, Janssen PM, Whitson BA, Mokadam NA, Biesiadecki BJ, Accornero F, Hummel
754 JD, Mohler PJ, Dobrzynski H, Zhao J and Fedorov VV. Impaired neuronal sodium channels cause intranodal
755 conduction failure and reentrant arrhythmias in human sinoatrial node. *Nat Commun*. 2020;11:512.
756 55. Lenning M, Fortunato J, Le T, Clark I, Sherpa A, Yi S, Hofsteen P, Thamilarasu G, Yang J, Xu X, Han HD,
757 Hsiai TK and Cao H. Real-Time Monitoring and Analysis of Zebrafish Electrocardiogram with Anomaly
758 Detection. *Sensors (Basel)*. 2017;18.
759 56. Sun X, Hoage T, Bai P, Ding Y, Chen Z, Zhang R, Huang W, Jahangir A, Paw B, Li YG and Xu X. Cardiac
760 hypertrophy involves both myocyte hypertrophy and hyperplasia in anemic zebrafish. *PLoS One*. 2009;4:e6596.
761 57. Glukhov AV, Kalyanasundaram A, Lou Q, Hage LT, Hansen BJ, Belevych AE, Mohler PJ, Knollmann BC,
762 Periasamy M, Gyorke S and Fedorov VV. Calsequestrin 2 deletion causes sinoatrial node dysfunction and atrial
763 arrhythmias associated with altered sarcoplasmic reticulum calcium cycling and degenerative fibrosis within
764 the mouse atrial pacemaker complex1. *Eur Heart J*. 2015;36:686-97.
765 58. Lang D and Glukhov AV. High-resolution Optical Mapping of the Mouse Sino-atrial Node. *J Vis Exp*.
766 2016.
767 59. Lang D, Sulkin M, Lou Q and Efimov IR. Optical mapping of action potentials and calcium transients in
768 the mouse heart. *J Vis Exp*. 2011.
769 60. Lang D, Glukhov AV, Efimova T and Efimov IR. Role of Pyk2 in cardiac arrhythmogenesis. *Am J Physiol*
770 *Heart Circ Physiol*. 2011;301:H975-83.

771 61. Love MI, Huber W and Anders S. Moderated estimation of fold change and dispersion for RNA-seq
772 data with DESeq2. *Genome Biol*. 2014;15:550.
773

Figure 1

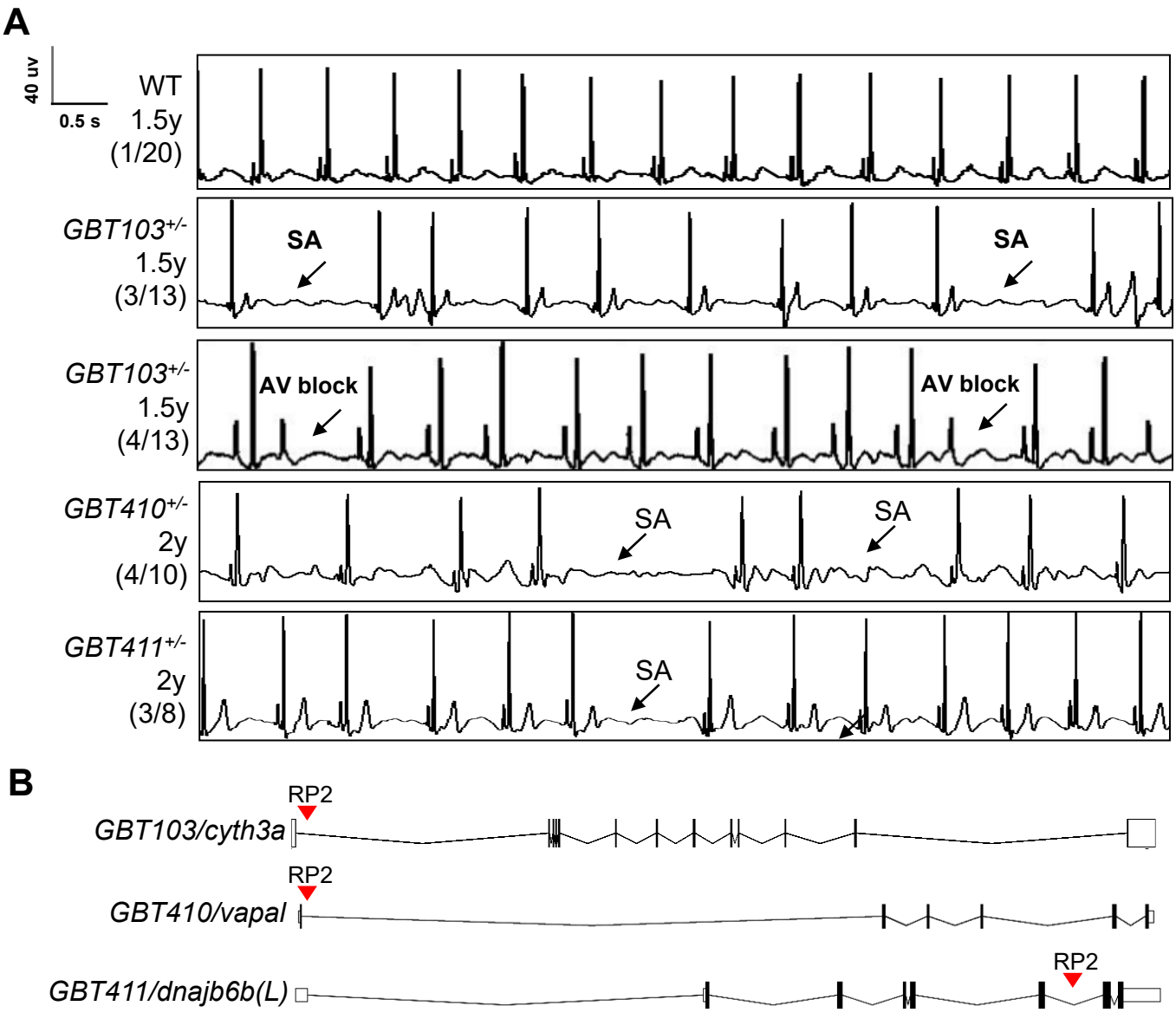

Figure 1. Screening of 35 ZIC lines identified 3 mutants with increased incidence of SA and/or AVB episodes

(A) Representative ECG recordings for 3 heterozygous GBT mutants with incidence of sinus arrest (SA) and/or atrioventricular block (AVB) episodes compared to WT control. **(B)** RP2 gene-break transposon insertional positions in the 3 candidate SSS mutants.

Figure 2

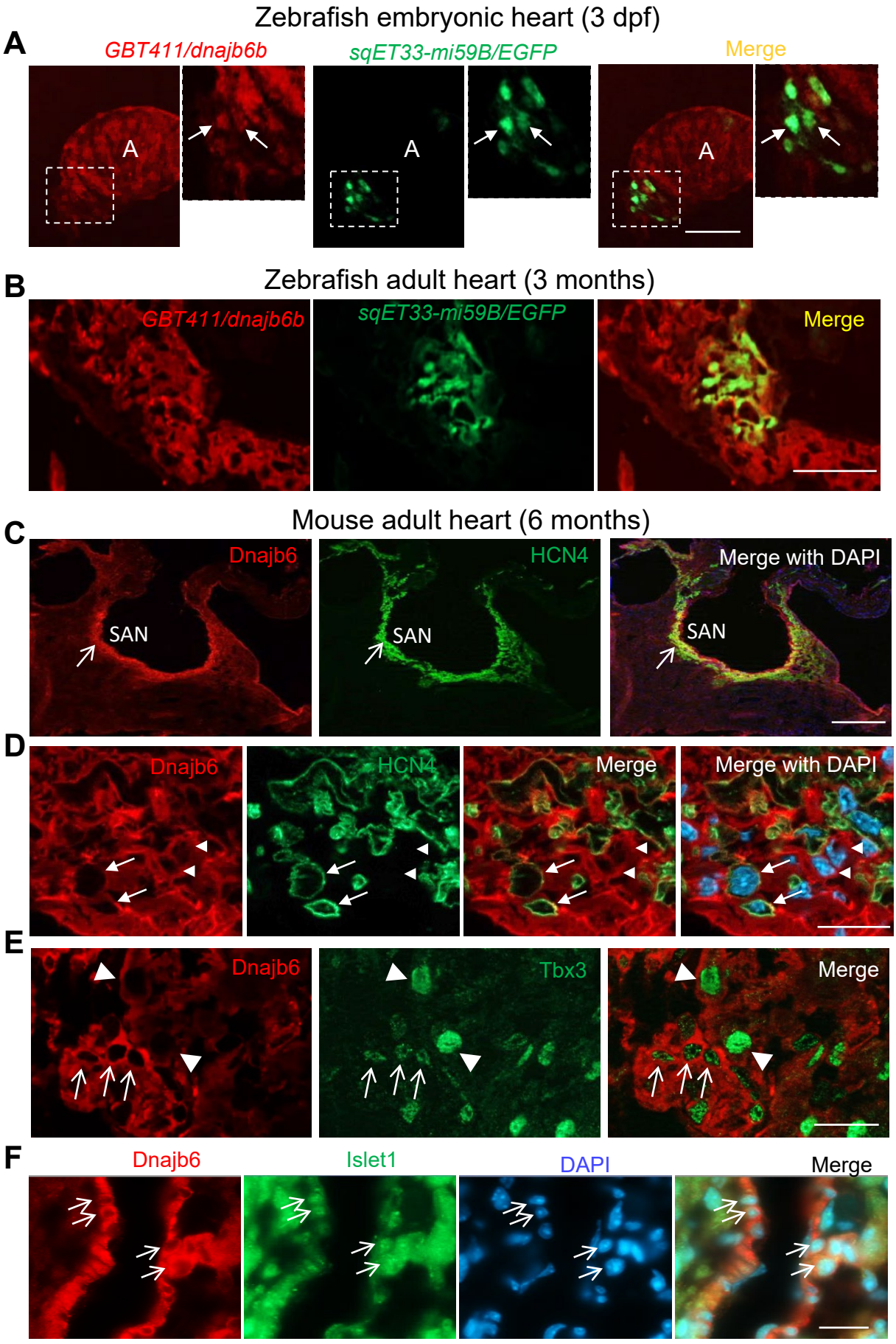
Zebrafish embryonic heart (3 dpf)
A
GBT411/dnajb6b
sqET33-mi59B/EGFP
Merge
A
A
A
Zebrafish adult heart (3 months)
B
GBT411/dnajb6b
sqET33-mi59B/EGFP
Merge
Mouse adult heart (6 months)
C
Dnajb6
HCN4
Merge with DAPI
SAN
SAN
SAN
D
Dnajb6
HCN4
Merge
Merge with DAPI
E
Dnajb6
Tbx3
Merge
F
Dnajb6
Islet1
DAPI
Merge

Figure 2. Dnajb6 is expressed in the SAN in both zebrafish and mouse
(A-B) Co-localization analysis of mRFP in *GBT411/dnajb6b* with the reporter line sqET33-mi59B in which EGFP labels cardiac conduction system (CCS) in zebrafish. The mRFP reporter for the *GBT411* tagged Dnajb6b protein partially overlaps with the EGFP reporter in the sqET33-mi59B transgenic line that labels the SAN in embryonic atrium at 3 dpf (A) and atrio-ventricular canal (AVC) in adult hearts (B). Arrows indicate EGFP+ cells in the sqET33-mi59B reporter line. A: atrium. V: ventricle. dpf, days post-fertilization. **(C)** The Dnajb6 antibody immunostaining signal largely overlapped with the HCN4 immunostaining signal in mouse SAN tissues under low magnification. **(D)** Under higher magnification, expression of Dnajb6 (red) only partially overlapped with HCN4 (green) as revealed by antibody co-immunostaining. Arrows point to cells with overlapping patterns. Arrowheads point to cells with no-overlapping. **(E)** Shown are images indicating expression of Dnajb6 protein largely overlapping with the Tbx3 antibody immunostaining with medium to low intensity, but not strong signal in the SAN tissues. Arrows point to cells with strong Tbx3 immunostaining signal. Arrowheads point to cells with medium to low level of Tbx3 immunostaining signal. **(F)** Shown are images indicating expression of Dnajb6 protein largely overlapping with the Islet1, a transcription factor labeling SAN cells. Arrows point to cells with overlapping immunostaining signal for both Dnajb6 and Islet1. Scale bars in A, C, 50 μm. Scale bars in B, D, E, F, 20 μm.

Figure 3

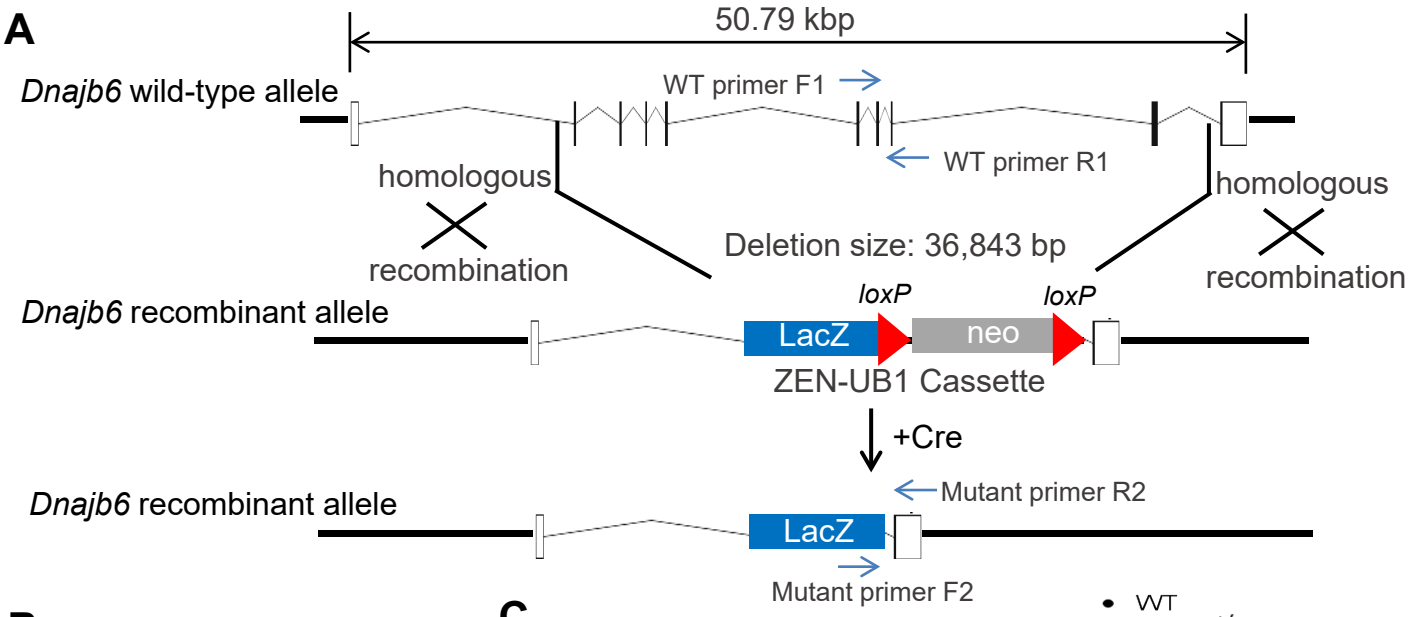
A
50.79 kbp
Dnajb6 wild-type allele
WT primer F1
WT primer R1
homologous
recombination
Deletion size: 36,843 bp
homologous
recombination
Dnajb6 recombinant allele
loxP
loxP
LacZ
neo
ZEN-UB1 Cassette
+Cre
Dnajb6 recombinant allele
Mutant primer R2
LacZ
Mutant primer F2

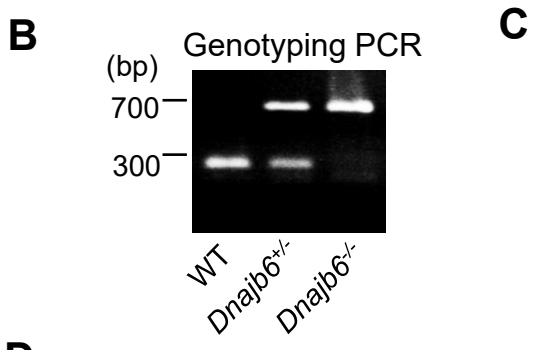
B
Genotyping PCR
(bp)
700
300
WT
Dnajb6+/-
Dnajb6-/-

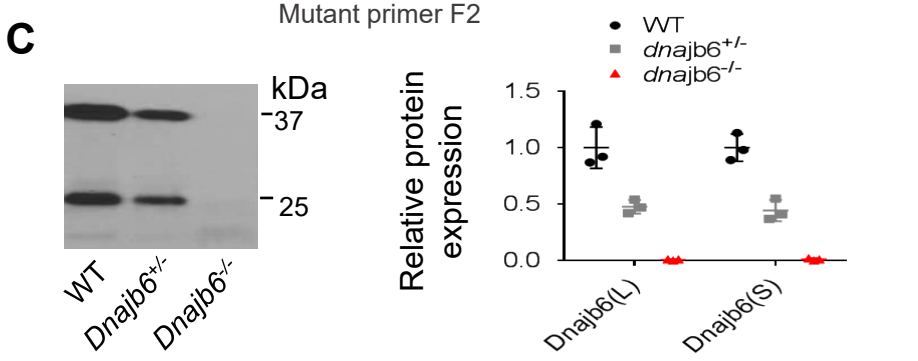
C
kDa
37
25
WT
Dnajb6+/-
Dnajb6-/-
WT
dnajb6+/-
dnajb6-/-
Relative protein expression
1.5
1.0
0.5
0.0
Dnajb6(L)
Dnajb6(S)

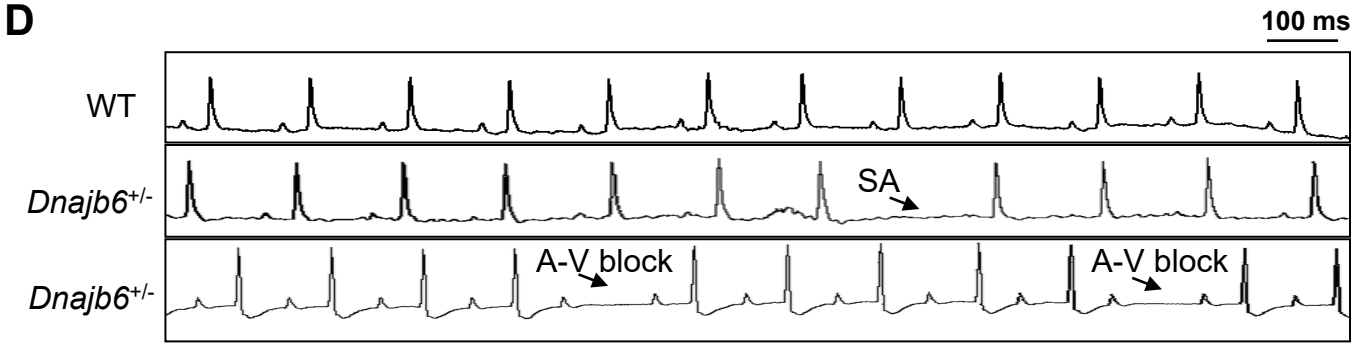
D
100 ms
WT
Dnajb6+/-
SA
Dnajb6+/-
A-V block
A-V block

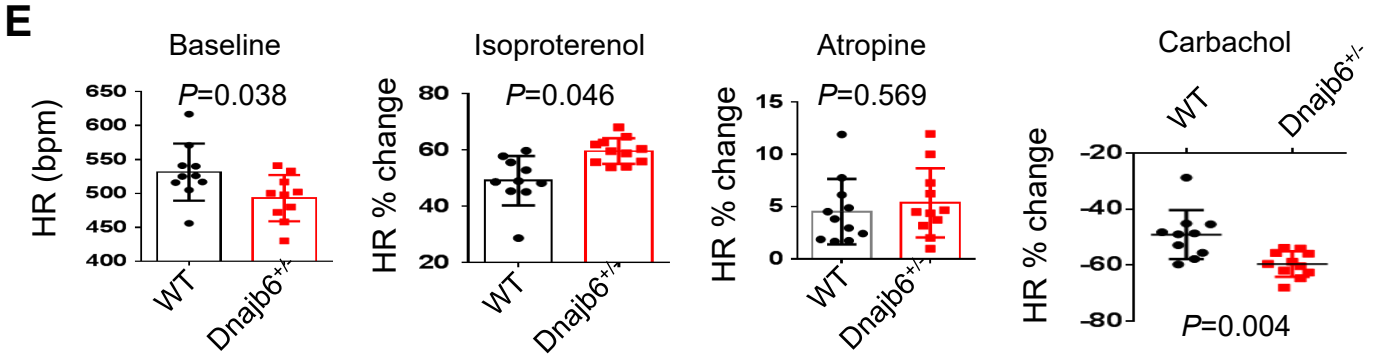
E
Baseline
HR (bpm)
650
600
550
500
450
400
P=0.038
WT
Dnajb6+/-
Isoproterenol
HR % change
80
60
40
20
P=0.046
WT
Dnajb6+/-
Atropine
HR % change
15
10
5
0
P=0.569
WT
Dnajb6+/-
Carbachol
HR % change
-20
-40
-60
-80
WT
Dnajb6+/-
P=0.004

Figure 3. *Dnajb6*$^{+/-}$ mice exhibited increased incidence of SA and AVB and impaired response to autonomic stimuli

(A) Schematics of the Dnajb6 knockout (KO) mice. The insertion of Velocigene cassette ZEN-Ub1 created a deletion of 36,843 bp nucleotides spanning from the first to the last intron of the *Dnajb6* gene at the Chromosome 5. The neomycin selection cassette was excised after crossed to a Cre expression line. **(B)** Representative DNA gel images of PCR genotyping for identifying WT (300 bp), *Dnajb6*$^{+/-}$ heterozygous (hets), and *Dnajb6*$^{-/-}$homozygous (homo) mutant alleles (700 bp). **(C)** Western blotting and quantification of Dnajb6 short (S) and long (L) protein expression in WT and *Dnajb6* mutants. N=3 animal per group. **(D)** Shown are representative ECG recordings results showing SA and AVB phenotypes detected in the *Dnajb6*$^{+/-}$ mice at 6 months. **(E)** The *Dnajb6*$^{+/-}$ mice manifests impaired response to different autonomic stimuli. N=10-12 mice per group. Unpaired student's *t*-test. SA, sinus arrest. AVB, atrioventricular block.

Figure 4

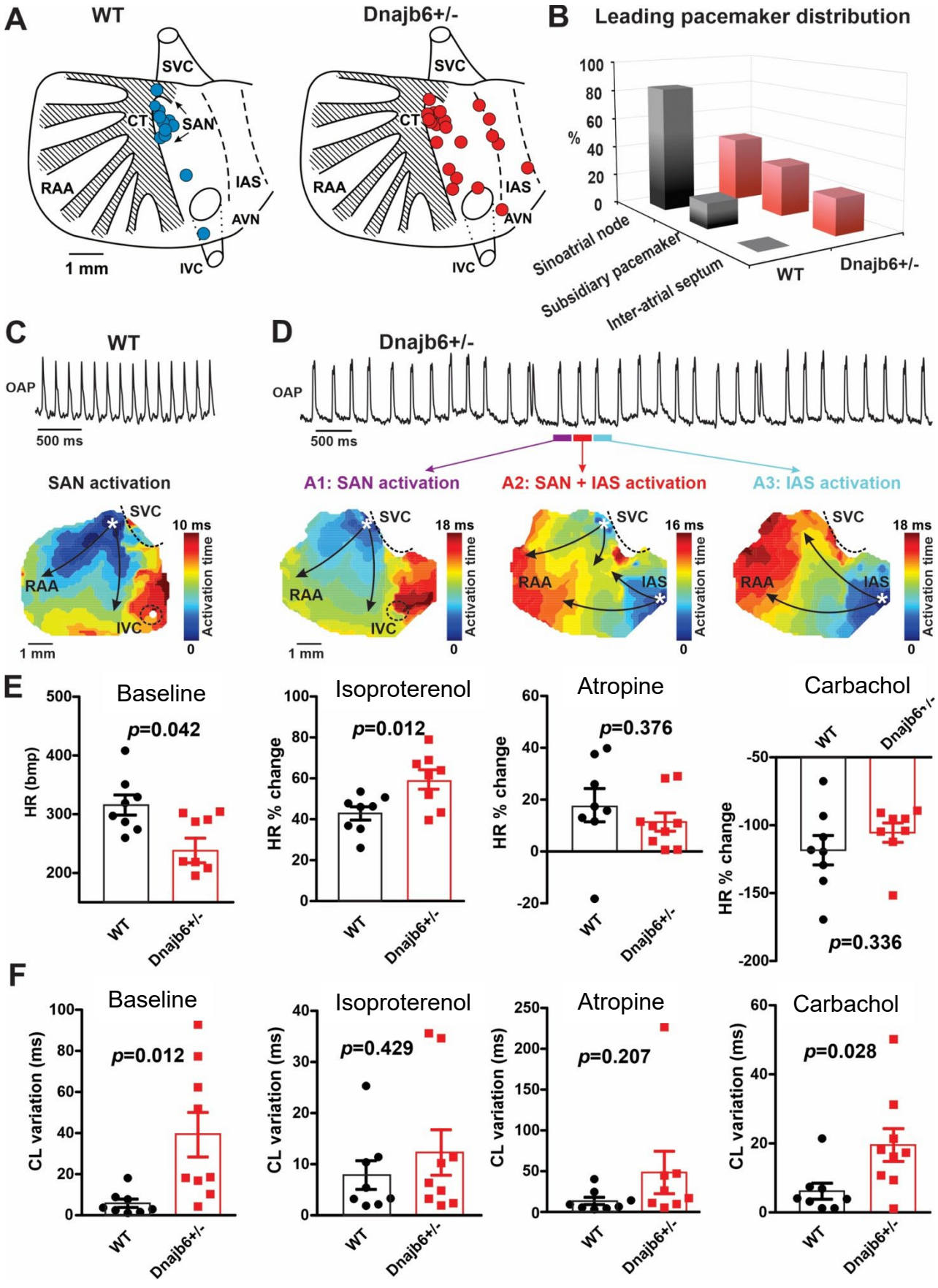
A
WT
Dnajb6+/-
SVC
CT
SAN
RAA
IAS
AVN
IVC
1 mm
B
Leading pacemaker distribution
100
80
60
40
20
0
%
Sinoatrial node
Subsidiary pacemaker
Inter-atrial septum
WT
Dnajb6+/-
C
WT
OAP
500 ms
SAN activation
SVC
10 ms
RAA
IVC
Activation time
0
1 mm
D
Dnajb6+/-
OAP
500 ms
A1: SAN activation
A2: SAN + IAS activation
A3: IAS activation
SVC
18 ms
RAA
IVC
Activation time
0
1 mm
SVC
16 ms
RAA
IAS
Activation time
0
SVC
18 ms
RAA
IAS
Activation time
0
E
Baseline
p=0.042
HR (bmp)
500
400
300
200
WT
Dnajb6+/-
Isoproterenol
p=0.012
HR % change
100
80
60
40
20
0
WT
Dnajb6+/-
Atropine
p=0.376
HR % change
60
40
20
0
-20
WT
Dnajb6+/-
Carbachol
WT
Dnajb6+/-
HR % change
-50
-100
-150
-200
p=0.336
F
Baseline
p=0.012
CL variation (ms)
100
80
60
40
20
0
WT
Dnajb6+/-
Isoproterenol
p=0.429
CL variation (ms)
40
30
20
10
0
WT
Dnajb6+/-
Atropine
p=0.207
CL variation (ms)
250
200
150
100
50
0
WT
Dnajb6+/-
Carbachol
p=0.028
CL variation (ms)
60
40
20
0
WT
Dnajb6+/-

Figure 4. SAN dysfunction in the *Dnajb6*$^{+/-}$ mice

(A) Leading pacemakers were located and plotted from both WT (blue dots) and *Dnajb6*$^{+/-}$ (red dots) mice. One mouse could have multiple leading pacemaker locations due to the competing pacemakers and ectopic activities. SVC and IVC, superior and inferior vena cava; RAA, right atrial appendage; CT, crista terminalis; IAS, inter-atrial septum; AVN, atrioventricular node. Distribution of the leading pacemakers is summarized in panel. **(B)** Majority of leading pacemakers located within the SAN area in WT whereas, in *Dnajb6*$^{+/-}$ mice, significant increase of leading pacemakers locating in subsidiary pacemaker area and IAS was observed. **(C-D)** Activation map based on the optical mapping of action potentials showed representative leading pacemaker locations in WT (SAN) and *Dnajb6*$^{+/-}$ mice (SAN and IAS areas). **(E)** Optical mapping on isolated atrial preparation showed bradycardia (baseline) and different responses of heart rate during isoproterenol, atropine, and carbachol stimulations between WT and *Dnajb6*$^{+/-}$ mice. N=7-9 mice per group. Unpaired student's *t*-test. **(F)** Increased cycle length (CL) variation was observed in *Dnajb6*$^{+/-}$ isolated atrial preparations during different autonomic stimulations. N=7-9 mice per group. Unpaired student's *t*-test.

Figure 5

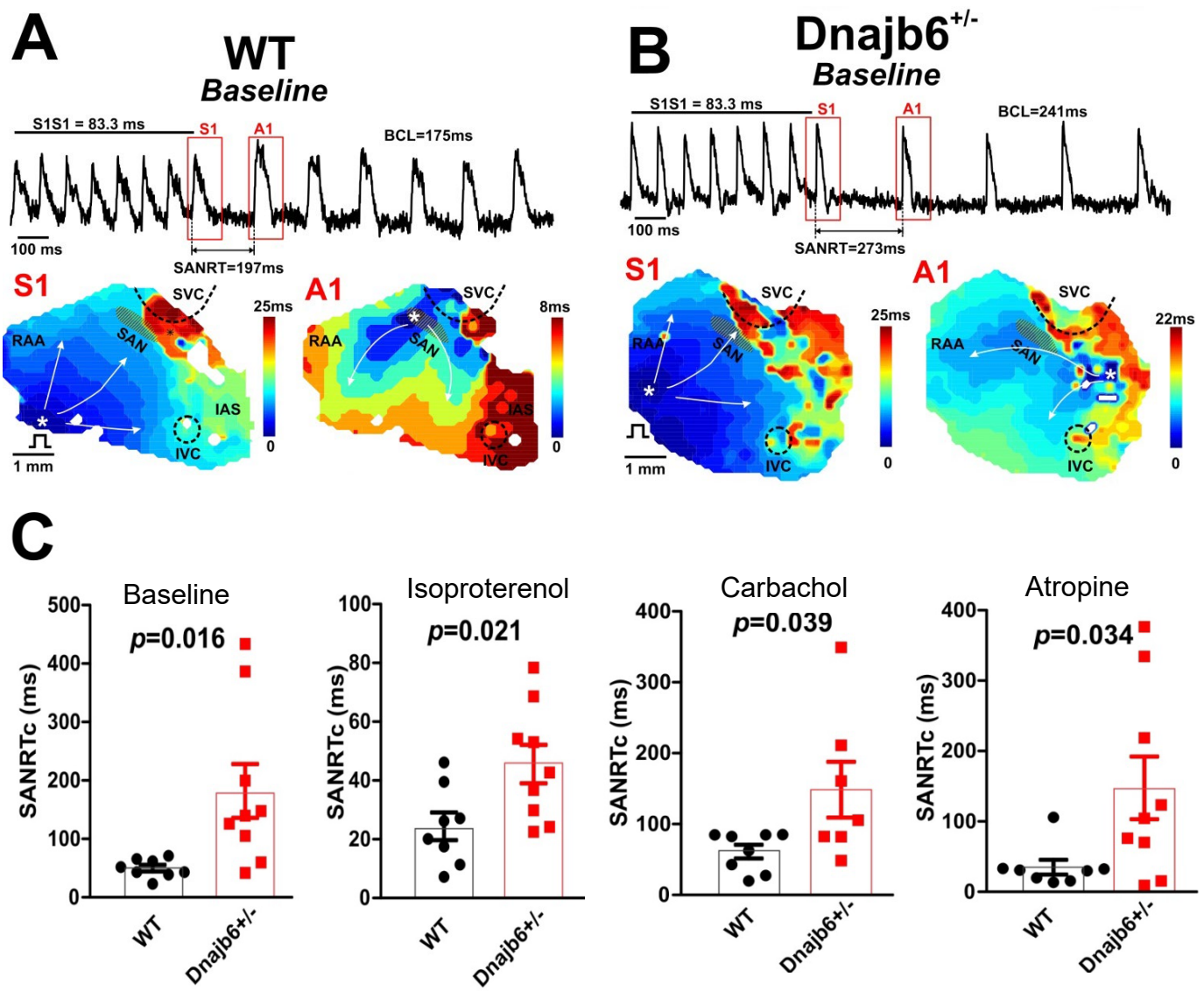

Figure 5. Sinus node recovery time was prolonged in the *Dnajb6*$^{+/-}$ mice
(A-B) Representative activation maps reconstructed for the last pacing stimulus (S1) and the first spontaneous post-pacing atrial beat (A1) during SAN recovery time (SANRT) measurements are shown. A site of the earliest atrial activation is labeled by a white asterisk. In *Dnajb6*$^{+/-}$ group, unlike WT, the first spontaneous post-pacing atrial beat (A1) originated from an ectopic location outside of the anatomically and functionally defined SAN area. **(C)** Summarized data for corrected SANRT (SANRTc) measured during different autonomic stimulations is shown. N=7-9 mice per group. Unpaired student's *t*-test.

Figure 6

A

Six calcium homeostasis and ion channel related DE genes

Ensemble ID	Gene	Protein	Log2 FC	*P* value	Gene Ontology/Function Annotation
ENSMUSG00000037996	*Slc24a2*	Solute Carrier Family 24 Member 2	1.27	0.000623	Cellular calcium ion homeostasis and calcium channel activity
ENSMUSG00000059742	*Kcnh7*	Potassium Voltage-Gated Channel Subfamily H Member 7	1.21	8.32E-06	Voltage-gated potassium channel activity
ENSMUSG00000050840	*Cdh20*	Cadherin 20	1.52	1.37E-06	Calcium ion binding and calcium-dependent cell-cell adhesion
ENSMUSG00000009687	*Fxyd5*	FXYD-domain containing ion transport regulator	-1.01	0.000376	Ion transport and sodium channel regulator activity
ENSMUSG00000020733	*Slc9a3r1*	Na(+)/H(+) exchange regulatory cofactor NHE-RF	-1.19	0.000253	Sodium/hydrogen exchanger regulatory cofactor
ENSMUSG00000042357	*Gjb5*	Gap junction protein			Gap junction channel activity

B

Four Wnt pathway related DE genes

Ensemble ID	*Gene*	Protein	Log2 FC	*P* value	Gene Ontology/Function Annotation
ENSMUSG00000032064	*Dixdc1*	Dishevelled/Axin domains 1 containing protein	1.00	1.77E-05	Regulator of Wnt signaling pathway
ENSMUSG00000010797	*Wnt2*	Wnt family member 2	-1.23	0.000159	Canonical Wnt signaling pathway
ENSMUSG00000018486	*Wnt9b*	Wnt family member 9B	-2.27	3.18E-05	Canonical Wnt signaling pathway
ENSMUSG00000070348	*Ccnd1*	G1/S-specific cyclin-D1	-1.03	0.000451	A direct target gene of Wnt signaling pathway

C

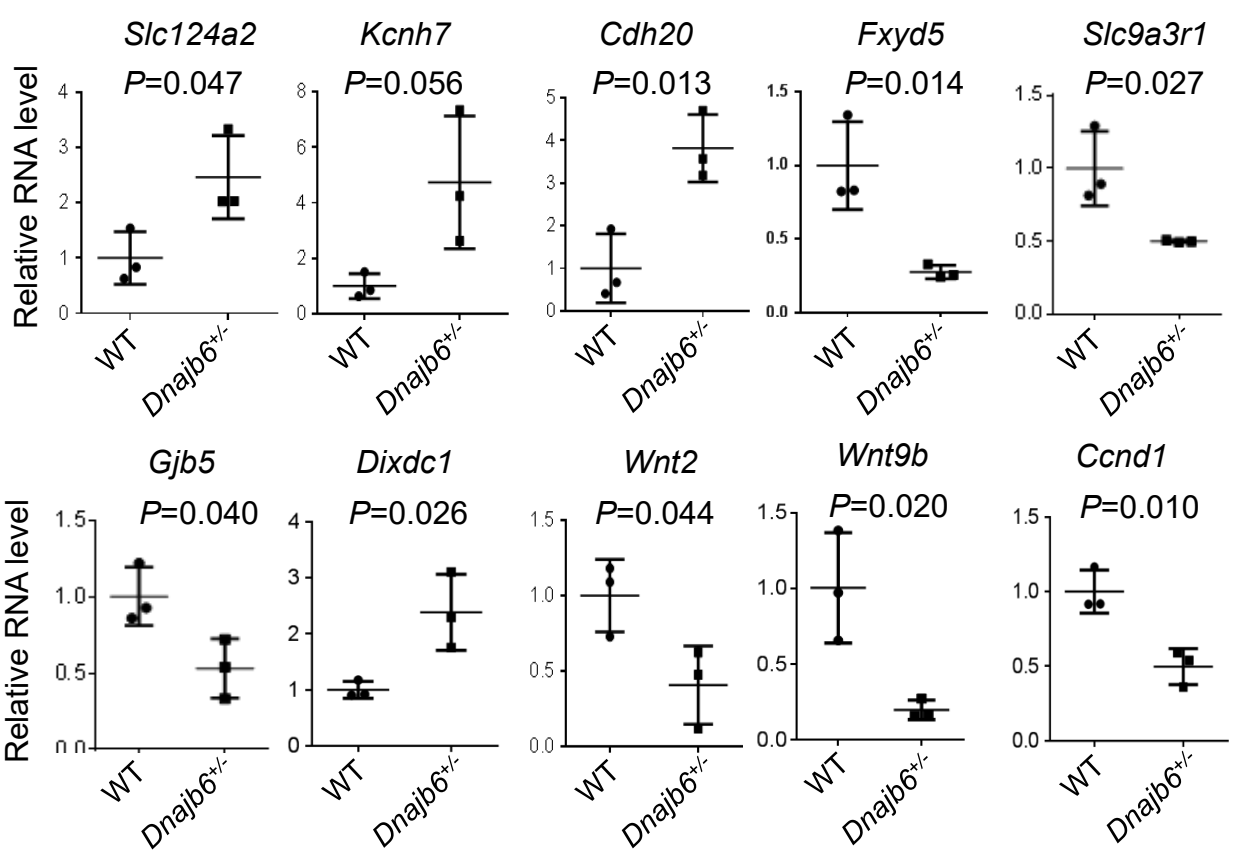

Figure 6. Transcriptomes are altered in the atrium of *Dnajb6*$^{+/-}$ mice
(A) Expression of six calcium homeostasis and ion channel related genes were altered in the *Dnajb6*$^{+/-}$ mice atrium. **(B)** Expression of four Wnt pathway related genes were altered in the *Dnajb6*$^{+/-}$ mice atrium. **(C)** Quantitative polymerase chain reaction (qPCR) validation of DE genes listed in A and B, normalized to Gapdh; RNA was extracted from an individual moue atrium, which was considered a single biological replicate. Samples were collected in triplicate. N=3 mice per group. Unpaired student's *t*-test.

Table 1. Collection of 35 zebrafish insertional cardiac (ZIC) mutants

GBT #	Gene ID	Human ortholog	Insertion position	OMIM#
GBT001	*casz1*	*CASZ1*	5' UTR	609895
GBT002	*sorbs2b*	*SORBS2*	1st intron	616349
GBT103	*cyth3a*	*CYTH3*	1st intron	605081
GBT130	*lrp1b*	*LRP1*	73rd intron	107770
GBT135	*bhlhe41*	*BHLHE41*	2nd intron	606200
GBT136	*ano5a*	*ANO5*	1st intron	608662
GBT145	*epn2*	*EPN2*	1st intron	607263
GBT166	*atp1b2a*	*ATP1B2A*	1st intron	182331
GBT235	*lrpprc*	*LRPPRC*	22nd intron	607544
GBT239	*map7d1b*	*MAP7D1*	1st intron	NA
GBT249	*b2ml*	*B2M*	1st intron	109700
GBT250	*ptprm*	*PTPRM*	1st intron	176888
GBT268	*idh2*	*IDH2*	12th intron	147650
GBT298	*zgc:194659*	*NA*	1st intron	NA
GBT270	*zpfm2a*	*ZFPM2*	2nd intron*	603693
GBT299	*dph1*	*DPH1*	1st intron	603527
GBT340	*nfatc3*	*NFATC3*	1st intron	602698
GBT345	*amot*	*AMOT*	1st intron	300410
GBT360	*tefm*	*TEFM*	1st intron	NA
GBT361	*abr*	*ABR*	3' UTR	600365
GBT364	*mat2aa*	*MAT2A*	1st intron	601468
GBT386	*babam1*	*BABAM1*	2nd intron	612766
GBT402	*scaf11*	*SCAF11*	2nd intron	603668
GBT410	*vapal*	*VAPA*	1st intron	605703
GBT411	*dnajb6b*	*DNAJB6*	6th intron*	611332
GBT412	*xpo7*	*XPO7*	1st intron	606140
GBT415	*arrdc1b*	*ARRDC1*	1st intron	NA
GBT416	*csrnp1b*	*CSRNP1*	1st intron*	606458
GBT419	*rxraa*	*RXRA*	1st intron*	180245
GBT422	*insrb*	*INSR*	6th intron	147670
GBT424	*v2rl1*	*VMN2R1*	2nd intron	NA
GBT425	*mrps18b*	*MRPS18B*	5th intron	611982
GBT503	*stat1a*	*STAT1*	6th intron*	600555
GBT513	*map2k6*	*MAP2K6*	1st intron	601254
GBT589	*oxsr1b*	*OXSR1*	3rd intron	604046

OMIM, Online Mendelian Inheritance in Man; NA, not available

Table 2. ECG quantification to validate 3 GBT lines as SA mutants in homozygous fish

Genotype	Age	N	SA incidence (%)	SA Frequency (epm)	Heart rate (bpm)
WT	16 m	20	5.0	2.0	100.1±11.1
GBT103$^{-/-}$	16 m	7	57.1*	3.4±2.9	89.1±18.8
GBT410$^{-/-}$	16 m	9	44.4*	1.4±0.6	99.9±17.7
GBT411$^{-/-}$	16 m	10	40.0*	3.0±1.0	90.6±7.5*

SA, sinus arrest. bpm, beats per minute. N=7-20. *, $P<0.05$, data are expressed as mean±SEM. For SA incidence comparison, Chi-square test. For heart rate comparison, unpaired student's *t*-test.

Table 3. Echocardiography indices in the *Dnajb6*$^{+/-}$ heterozygous mice compared to WT controls at 1 year

	WT	*Dnajb6*$^{+/-}$	*P* value
Mice number (n)	6	6	
HR (bpm)	481±16	447±11	0.0017
IVSd (mm)	0.73±0.08	0.80±0.06	0.0895
LVIDd (mm)	3.92±0.33	3.71±0.18	0.2022
LVPWd (mm)	0.80±0.05	0.81±0.03	0.5204
IVSs (mm)	1.10±0.0.07	1.11±0.08	0.7878
LVIDs (mm)	2.95±0.26	2.77±0.15	0.1821
LVPWs (mm)	1.11±0.06	1.21±0.12	0.1000
LVEF (%,Cube)	57.17±5.95	58.17±3.92	0.7380
LVEF (%, Teich)	55.50±5.82	56.67±4.23	0.6996
LVFS (%)	24.67±3.61	25.17±2.32	0.7813
LVd Mass (g)	0.69±0.01	0.68±0.01	0.7650
LVs Mass (g)	0.69±0.01	0.69±0.01	1.0000

HR, heart rate; bpm, beats per minute; IVSd, Interventricular septum thickness at end–diastole; LVIDd, left ventricular internal dimension at end-diastole; LVPWd, left ventricular internal dimension at end-diastole; IVSs, Interventricular septum thickness at end–systole; LVIDs, Left ventricular internal dimension at end-systole; LVPWs, Left ventricular posterior wall thickness at end–diastole; LVEF, left ventricular ejection fraction; LVFS, left ventricular fractional shortening; LVd, left ventricular at end-diastole; LVs, left ventricular at end-systole. Unpaired 2-tailed student's *t*-test.

Table 4. ECG quantification of *Dnajb6* heterozygous mice at 6 months of age

Genotype	Age	N	SA incidence (%)	AVB incidence (%)	Heart rate (bpm)
WT	6 m	20	5.0	0	516.3±34.3
Dnajb6+/-	6 m	44	34.1*	6.8	494.8±38.3*

SA, sinus arrest. bpm, beats per minute. N=20-44. *, $P<0.05$, data are expressed as mean±SEM. For SA incidence comparison, Chi-square test. For heart rate comparison, unpaired student's *t*-test.